AMAS COURSE ON RANDOM MATERIAL MICROSTRUCTURES
RMM'04 – (PP.49–99) – WARSAW, FEBRUARY 2-4, 2004

Stochastic characterization of material microstructure with application to fracture

S. R. ARWADE

Dept. of Civil Engineering
The Johns Hopkins University
3400 N. Charles St.
Baltimore, MD 21218

These notes contain the contents of four lectures delivered at the Random Material Microstructures workshop held at the Centre of Excellence for Advanced Materials and Structures, Warsaw, Poland. The lectures cover the following topics: (1) statistical characterization of random heterogeneous microstructures, (2) probabilistic models and sample generation for polycrystalline materials, (3) probabilistic models and sample generation for multi-phase materials, and (4) application of probabilistic material models to problems in small scale fracture.

1. Data types and statistical characterization

In attempting to develop probabilistic models for material microstructures, and implement them for application to problems in solid mechanics such as fracture, the modeler/analyst must at all times base the approach on physical reality. The physical reality to which the analyst of heterogeneous material microstructures must refer is the set of properties and features of the material microstructures which can be measured experimentally.

These notes address two broad classes of materials, composites and polycrystals. These two encompass most of the materials commonly used in engineering applications today. In this section we concentrate on the types of data which are available experimentally for each of these two classes of materials, and a discussion of the types of statistical quantities which can be derived from the experimental data. It is these statistical quantities which will be used to motivate and calibrate the probabilistic material models which will be presented in the second and third sections. This section is organized into two main parts:

1. general statistical quantities, and
2. material specific statistical quantities.

1.1. General statistical quantities

The most general means of representing a material microstructure in a given domain S is as a function which describes some property of the material at all points in S. Since we concern ourselves primarily with *random, heterogeneous* materials here, this function must be considered random. Therefore, for the remainder of these notes, the random field will be adopted as the preferred representation for random material microstructures. In its most general form we denote this random field by $\mathbf{Y}(\mathbf{x})$ where $\mathbf{Y} \in \mathbb{R}^n$ is the, possibly vector valued, random field, and $\mathbf{x} \in \mathbb{R}^m$ is a point in S, which is m-dimensional. This random vector field representation can be made to describe the material microstructure in as great a degree of detail as desired.

Example 1. The microstructure of concrete can be represented by the random vector field

$$\mathbf{Y}(\mathbf{x}) = [D(\mathbf{x}), E(\mathbf{x})]^T \tag{1.1}$$

where $\mathbf{x} \in \mathbb{R}^3$ is a position vector, and D and E are the density and elastic modulus respectively of the material at $\mathbf{x}$. The random field can take values in an interval of the real line to capture the highly detailed variation of the local material properties, or, alternatively, concrete can be considered a three phase composite, in which the phases are the aggregate, the cement paste, and voids. In this case the random field $\mathbf{Y}(\mathbf{x})$ can take only three distinct values depending on which phase includes $\mathbf{x}$.

Example 2. The crystallographic orientation of a crystalline solid can be described by the vector of three Euler angles $[\phi_1, \Phi, \phi_2]$. The orientation can in turn be used to derive the anisotropic constitutive law for the local microstructure. Thus, the random field representation

$$\mathbf{Y}(\mathbf{x}) = [\phi_1(\mathbf{x}), \Phi(\mathbf{x}), \phi_2(\mathbf{x})]^T \tag{1.2}$$

with $\mathbf{x} \in \mathbb{R}^3$ defines the microstructure of a three dimensional polycrystal with enough fidelity that grain geometry and material properties can be inferred.

Example 3. Thin filamentous materials can sometimes be modelled as one dimensional. For the purposes of a model useful in linear elastic analysis, an appropriate random field representation for such a microstructure would be

$$Y(x) = E(x) \tag{1.3}$$

where $x \in \mathbb{R}$ represents the position along the length of the material.

1.1.1. Densities, distributions and moments. We now proceed from our understanding of material microstructures as an example of a random field to develop some statistical quantities which can be used to describe the microstructure. These will all correspond to probabilistic quantities describing the random field, the intention being that the statistics can be estimated from experimental data in order to calibrate the random field models.

These notes are meant to be self contained, and therefore we begin with some elementary descriptors of the random field. The descriptors are defined in as much detail as necessary for conceptual understanding. For more detailed definitions the reader should consult any of several appropriate texts on probability, statistics, and random processes/fields [10, 15, 18, 33].

The *joint marginal cumulative distribution function* of the random field is denoted by $F(\mathbf{y}, \mathbf{x})$, a function which is monotonically non-decreasing in any of the y_i directions, and satisfies the limiting conditions $\lim_{\mathbf{y}\to\infty} F(\mathbf{y}, \mathbf{x}) = 1$ and $\lim_{\mathbf{y}\to-\infty} F(\mathbf{y}, \mathbf{x}) = 0$. This function can be defined in terms of a probability statement by

$$F(\mathbf{y}, \mathbf{x}) = P[Y_1(\mathbf{x}) \leq y_1, \ldots, Y_n(\mathbf{x}) \leq y_n] \tag{1.4}$$

at point $\mathbf{x}$. The same information is contained in the *joint marginal probability density function* $f(\mathbf{y}, \mathbf{x})$ which is always non-negative and satisfies

$$\int_{-\infty}^{\infty} \cdots \int_{-\infty}^{\infty} f(\mathbf{y}, \mathbf{x}) dy_1 \ldots dy_n = 1. \tag{1.5}$$

Each of these functions is here given as depending upon position $\mathbf{x}$ to indicate that the local statistical properties of the microstructure can vary with position. When $\mathbf{y} \in \mathbb{R}^n$, $n > 1$, the marginal cdf and pdf are *joint* distribution and density functions respectively. It can be prohibitive to obtain sufficient data to arrive at confident estimates of the joint density and distribution functions if the microstructure is to be characterized by a multivariate random vector. It can also be difficult to efficiently generate realizations from such multivariate joint density functions. For those reasons a reduced description of the density and distribution functions is often utilized, the *marginal distributions* and *densities*. The marginal distribution and density give the probability law of the individual components of $\mathbf{Y}(\mathbf{x})$ independent of the other components. The marginal density functions are determined from the joint density function by

$$f_i(y, \mathbf{x}) = \int_{-\infty}^{\infty} f(\mathbf{y}, \mathbf{x}) dy_1 \ldots dy_{i-1}\, dy_{i+1} \ldots dy_n. \tag{1.6}$$

In practice the marginal densities are directly estimated from experimental data rather than derived from the joint densities.

Probability density and cumulative distribution functions give information about the random character of a material microstructure at a particular point. In heterogeneous materials, however, spatial characteristics of the randomness may be more important than the pointwise random characteristics. For example, when considering the problem of flow through a porous medium, the connectivity of the void phase is more important than the volume fraction of the void phase in determining permeability.

In characterizing the spatial variability of microstructures we concentrate first on the correlation and covariance functions of the random field $\mathbf{Y}(\mathbf{x})$. The *correlation function* is defined by

$$\mathbf{r}(\mathbf{x}, \mathbf{z}) = E[\mathbf{Y}(\mathbf{x})\mathbf{Y}(\mathbf{z})^T] \tag{1.7}$$

where $\mathbf{x}$, $\mathbf{z}$ are position vectors and $E[\cdot]$ is the expectation operator so that $r_{ij}(\mathbf{x}, \mathbf{z}) = E[Y_i(\mathbf{x})Y_j(\mathbf{z})]$. By removing the mean from the computation of the correlation function one obtains the *covariance function*

$$\mathbf{c}(\mathbf{x}, \mathbf{z}) = E[(\mathbf{Y}(\mathbf{x}) - \boldsymbol{\mu}(\mathbf{x}))(\mathbf{Y}(\mathbf{z}) - \boldsymbol{\mu}(\mathbf{z}))^T] \tag{1.8}$$

where $\boldsymbol{\mu}(\mathbf{x}) = E[\mathbf{Y}(\mathbf{x})]$ is the vector of mean values of $\mathbf{Y}(\mathbf{x})$. Lastly we define the *normalized covariance function*, also referred to as the *scaled covariance function* which has components

$$\rho_{ij}(\mathbf{x}, \mathbf{z}) = \frac{c_{ij}(\mathbf{x}, \mathbf{z})}{\sigma_i(\mathbf{x})\sigma_j(\mathbf{z})} \tag{1.9}$$

where σ_i, σ_j are components of the vector of standard deviations of $\mathbf{Y}(\mathbf{x})$. The normalized covariance function takes values between -1 and 1. The component $c_{ij}(\mathbf{x}, \mathbf{z})$ gives the degree of linear dependence between the random variables $Y_i(\mathbf{x})$ and $Y_j(\mathbf{z})$. It is important at all times to recognize that lack of correlation does not imply independence of the random variables.

Example 4. The random variables $X \sim N(0, 1)$ and $Y = X^2$ are not independent since Y has a functional dependence upon X. The covariance of the two random variables,

$$E[X(Y - 1)] = E[XY] - E[X] = E[X^3] - E[X] = 0 \tag{1.10}$$

since the third moment of a standard normal variable is zero. These random variables are said to be uncorrelated, but are not independent.

With the statistical descriptors defined thus far it is possible to describe several packages of quantities which can form partial probabilistic characterizations of the material microstructure.

1. The *second moment description* consists of the means $\boldsymbol{\mu}(\mathbf{x})$ and the correlation function $\mathbf{r}(\mathbf{x}, \mathbf{z})$.
2. These can be augmented with the marginal distributions $F_i(y, \mathbf{x})$ or
3. when possible, with the joint marginal distribution $F(\mathbf{y}, \mathbf{x})$.

The second of these descriptions, combining the second moment properties with the marginal distributions, provides a rich characterization of the microstructure through the use of quantities which can typically be easily estimated from experimental data. The drawback of these characterizations is that they provide only a partial description of the microstructure's probabilistic character. A full description can be obtained only by determination of all of the *finite dimensional distributions* $F(\mathbf{y}_1, \ldots, \mathbf{y}_l; \mathbf{x}_1, \ldots, \mathbf{x}_l)$ of the random field. Collection of this information is impractical, and so, in analysis and modelling, a reduced characterization must always be employed.

In all of the preceding we have included a positional dependence in the notation, for example, $F(\mathbf{y}, \mathbf{x})$ for the cdf and $\mathbf{r}(\mathbf{x}, \mathbf{z})$ for the correlation function. This notation implies the assumption that the random field is non-stationary, that is, its probability law varies with position. In many microstructural modelling situations it is appropriate to assume the microstructure to be statistically stationary. A rigorous application of the concept of stationarity requires that all of the finite dimensional distributions of the random field are invariant under translations. This concept of stationarity need not be applied in its entirety in order to significantly simplify the statistical characterization of the microstructure. If we assume stationarity with respect to the marginal distributions and densities, and the covariance and correlation functions, the following simplifications can be made:

$$\begin{aligned} f(\mathbf{y}, \mathbf{x}) &= f(\mathbf{y}), \\ F(\mathbf{y}, \mathbf{x}) &= F(\mathbf{y}), \\ \boldsymbol{\mu}(\mathbf{x}) &= \boldsymbol{\mu}, \\ \boldsymbol{\sigma}(\mathbf{x}) &= \boldsymbol{\sigma}, \\ \mathbf{r}(\mathbf{x}, \mathbf{z}) &= \mathbf{r}(\mathbf{d}), \\ \mathbf{c}(\mathbf{x}, \mathbf{z}) &= \mathbf{c}(\mathbf{d}), \\ \boldsymbol{\rho}(\mathbf{x}, \mathbf{z}) &= \boldsymbol{\rho}(\mathbf{d}), \end{aligned} \tag{1.11}$$

where $\mathbf{d}$ is a vector of separation.

A further simplification can be made to the correlation and covariance functions if the field is assumed to be isotropic. In this case, the correlation function depends not on a vector of separation but only on a separation distance, so that $\mathbf{r}(\mathbf{d}) \rightarrow \mathbf{r}(d)$, and similarly for the covariance and scaled covariance functions.

As mentioned above, the second moment characterization of the microstructure random field may not provide sufficient characterization for a particular mechanics application. Since estimation of the finite dimensional distributions is prohibitively time consuming in many cases, higher order moments of the field may be used to further characterize the microstructure. For example, the third order correlation function is typically the next statistical quantity considered after the standard correlation and covariance functions. The third order correlation function of a random field is given by

$$\zeta_{ijk}(\mathbf{u}, \mathbf{v}, \mathbf{w}) = E[Y_i(\mathbf{u})Y_j(\mathbf{v})Y_k(\mathbf{w})] \tag{1.12}$$

where $\mathbf{u}$, $\mathbf{v}$, $\mathbf{w}$ are position vectors. The third order correlation function provides statistical information about the relationship between field values at three points in the microstructure. If the field is assumed to be stationary then $\zeta_{ijk}(\mathbf{u}, \mathbf{v}, \mathbf{w}) \rightarrow \zeta_{ijk}(\mathbf{d}_{12}, \mathbf{d}_{13}, \mathbf{d}_{23})$, and if it is isotropic then $\zeta_{ijk}(\mathbf{u}, \mathbf{v}, \mathbf{w}) \rightarrow \zeta_{ijk}(d_{12}, d_{13}, d_{23})$. While higher order correlation functions do contain additional statistical information about the microstructure, generation of material samples which match even a specified third order correlation function is an open topic of research [19].

1.1.2. N-point probability functions. To this point we have concentrated on statistical characterizations which are essentially standard in the random fields and processes community. We will now devote some attention to a set of statistical quantifiers which are commonly employed in the materials characterization community, the *n-point correlation functions* also called the *n-point probability functions.*

We will introduce the concept of the n-point probability function through the example of a composite material consisting of two or more distinct phases. Once the n-point probability functions are defined for such materials, the concept is extended to polycrystalline materials. A more detailed description of the n-point probability functions is given in [35].

For a composite material with m phases the microstructure can be described by a set of random fields which are the indicator functions $I_i(\mathbf{x})$ which obey $I_i(\mathbf{x}) = 1$ if $\mathbf{x}$ lies in phase i and $I_i(\mathbf{x}) = 0$ otherwise, and satisfy $\sum_{i=1}^{n} I_i(\mathbf{x}) = 1$, $\forall \mathbf{x} \in S$. In general, $n-1$ such random fields are necessary to completely define the composite microstructure if n phases are present.

Example 5. For a two phase composite such as that shown in Fig. 1, the microstructure is completely defined by the indicator function $I_1(\mathbf{x})$ since the indicator function for phase two can be determined by $I_2(\mathbf{x}) = 1 - I_1(\mathbf{x})$.

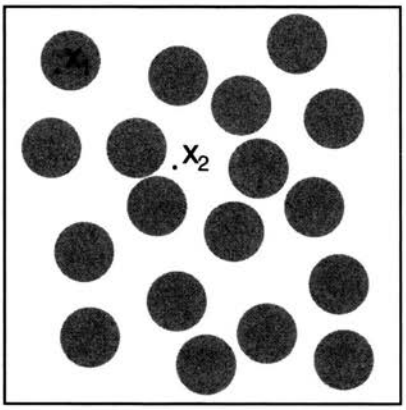

FIGURE 1. Two phase composite consisting of non overlapping disks. The microstructure can be described by the indicator function so that $I_1(x_1) = 1$ and $I_1(x_2) = 0$ if the disks are considered phase 1.

For a two phase composite such as that defined in the previous example, the 1-point probability function of phase i is

$$S_i^{(1)}(\mathbf{x}) = E[I_i(\mathbf{x})] = P[I_i(\mathbf{x}) = 1] \tag{1.13}$$

which gives the probability of finding phase i at location $\mathbf{x}$. The 1-point probability function can also be thought of as giving the volume fraction ϕ_i of phase i at location $\mathbf{x}$ provided we think of the volume fraction in an ensemble sense.

Following on the simple example of the 1-point probability function, the n-point probability function is defined to be

$$S_i^{(n)}(\mathbf{x}_1, \ldots, \mathbf{x}_n) = E[I_i(\mathbf{x}_1) \times \cdots \times I_i(\mathbf{x}_n)] \tag{1.14}$$

which, since quantity in brackets is zero unless $I_i(\mathbf{x}_j) = 1$, $1 \leq j \leq n$, also represents

$$P[I_i(\mathbf{x}_1) = 1, \ldots, I_i(\mathbf{x}_n) = 1], \tag{1.15}$$

the probability that all points $\mathbf{x}_i$, $i = 1, \ldots, n$ lie in phase i. The geometric interpretation of the 3-point probability function is given in Fig. 2 where the case is shown in which $I_1(\mathbf{x}_1) = I_1(\mathbf{x}_2) = I_1(\mathbf{x}_3) = 1$ if the inclusions are phase one.

As the indicator random field for phase 1 provides information regarding the phase 2 indicator function, so the n-point probability functions of phase

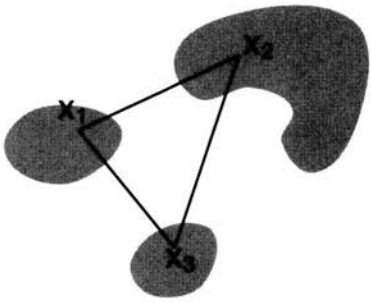

FIGURE 2. The 3-point probability function gives the probability that all three vertices of a triangle will lie in a particular phase of the composite material.

1 provide information about the corresponding phase 2 functions. Generally,

$$\begin{aligned} S_2^{(n)}(\mathbf{x}_1,\ldots,\mathbf{x}_n) &= E[\prod_{j=1}^{n} I_2(\mathbf{x}_j)] \\ &= E[\prod_{j=1}^{n}(1-I_1(\mathbf{x}_j))] \\ &= 1-\sum_{j=1}^{n} S_1^{(1)}(\mathbf{x}_j)+\sum_{j<k}^{n} S_1^{(2)}(\mathbf{x}_j\mathbf{x}_k) \\ &\quad -\sum_{j<k<l}^{n} S_1^{(3)}(\mathbf{x}_j,\mathbf{x}_k,\mathbf{x}_l)+\cdots+(-1)^n S_1^{(n)}(\mathbf{x}_1,\ldots,\mathbf{x}_n). \end{aligned} \tag{1.16}$$

Similarly we might be interested in a two point function which combines information about the phases,

$$\begin{aligned} S_{12}^{(2)}(\mathbf{x}_1,\mathbf{x}_2) &= E[I_1(\mathbf{x}_1)(1-I_1(\mathbf{x}_2))] \\ &= S_1^{(1)}(\mathbf{x}_1)-S_1^{(2)}(\mathbf{x}1,\mathbf{x}_2). \end{aligned} \tag{1.17}$$

Just as for the density, distribution and correlation/covariance functions, the n-point probability functions can be simplified by assumptions regarding stationarity and isotropy. For a stationary, isotropic microstructure, the 2-point probability function becomes $S_i^{(2)}(d_{12})$ where d_{12} is a separation distance. In cases where stationarity and isotropy are valid assumptions, the n-point probability functions up to $n=3$ can be estimated by examination of a planar section of a given material microstructure. This means that in practice these functions can be estimated from the types of micrographic

images which are commonly available. Estimation of higher order probability functions requires high fidelity three dimensional images of the material microstructure which are only now becoming commonly available through techniques such as CT scanning and magnetic resonance imaging [22].

The 2- and 3- point probability functions have limiting properties which are of interest, and quantify important features of the microstructure. For the 2-point probability function,

$$\begin{aligned} \lim_{d_{12}\to 0} S_i^{(2)}(d_{12}) &= \phi_i, \\ \lim_{d_{12}\to \infty} S_i^{(2)}(d_{12}) &= \phi_i^2, \end{aligned} \tag{1.18}$$

where ϕ_i is the volume fraction of phase i. For the 3-point function,

$$\begin{aligned} \lim_{d_{12}\to 0, d_{13},\to 0} S_i^{(3)}(d_{12}, d_{13}, d_{23}) &= \phi_i, \\ \lim_{d_{23}\to 0} S_i^{(3)}(d_{12}, d_{13}, d_{23}) &= S_i^{(2)}(d_{12}), \\ \lim_{d_{13}\to \infty, d_{12}\text{fixed}} S_i^{(3)}(d_{12}, d_{13}, d_{23}) &= \phi_i S_i^{(2)}(d_{12}), \\ \lim_{d_{ij}\to \infty} S_i^{(3)}(d_{12}, d_{13}, d_{23}) &= \phi_i^3. \end{aligned} \tag{1.19}$$

The above relations hold for the various permutations of the indices on the separation distances d_{ij}.

One final property of the 2-point correlation function is its relation to the standard correlation function as introduced earlier. For a two phase microstructure which is represented by its phase 1 indicator function so that $Y(\mathbf{x}) = I_1(\mathbf{x})$,

$$S_1^{(2)}(\mathbf{x}, \mathbf{z}) = E[I_1(\mathbf{x})I_1(\mathbf{z})] = E[Y(\mathbf{x})Y(\mathbf{z})] = r(\mathbf{x}, \mathbf{z}). \tag{1.20}$$

That is, the 2-point probability function and the standard spatial correlation function are equivalent. For materials with more than two phases relationships exist between the n-point probability functions and the spatial correlation functions, but they quickly become complicated.

We have so far based our definition of the n-point probability functions on composite materials with distinct phases. This has simplified the introduction of the idea of these functions since the random field describing the composite takes discrete values. The remaining question then is how to define the n-point probability functions for materials whose random field descriptions have continuous pdfs.

The example we concentrate on is that of a polycrystalline material [2]. A possible random field description of a polycrystalline material is

$$\mathbf{Y}(\mathbf{x}) = [\Psi_1, \Psi_2, \Psi_3]^T \tag{1.21}$$

where the substitution $\phi_1 \rightarrow \Psi_1$, $\Phi \rightarrow \Psi_2$, $\phi_2 \rightarrow \Psi_3$ has been made for the Euler angles to simplify the notation. Given this description of the polycrystalline microstructure, the 1-point probability function becomes

$$S^{(1)}(\mathbf{x}) = f(\mathbf{y}, \mathbf{x}), \tag{1.22}$$

or, simply, the probability density function of the crystallographic orientation. This function is commonly referred to as the *orientation distribution function*, or ODF. The 2-point function then becomes

$$S^{(2)}(\mathbf{x}, \mathbf{z}) = f(\mathbf{y}_1, \mathbf{y}_2; \mathbf{x}_1, \mathbf{x}_2) \tag{1.23}$$

which is a 12 dimensional joint probability density function for the orientation at two points $\mathbf{x}$, $\mathbf{z}$. Even if stationarity and isotropy is assumed, so that $S^{(2)}(\mathbf{x}, \mathbf{z}) = f(\mathbf{y}_1, \mathbf{y}_2; \mathbf{x}_1, \mathbf{x}_2) \rightarrow S^{(2)}(\mathbf{x}, \mathbf{z}) = f(\mathbf{y}_1, \mathbf{y}_2; d_{12})$ we are left with a 7 dimensional pdf. Estimation of a pdf of such high dimension is experimentally very difficult. While investigators have made such estimates for the 2-point function, estimation of the 3-point function, which is 12 dimensional under the assumptions of stationarity and isotropy seems impractical given the current state of experimental observation of polycrystalline microstructures. For this reason we take recourse primarily to a characterization of polycrystals consisting of the second moment properties and marginal distribution functions of the orientation.

1.2. Polycrystal statistical quantities

The statistical quantities introduced thus far are general in that they can be calculated for any microstructure which can be represented by a random field. When discussing polycrystalline microstructures, however, one further set of statistics can be quite important those that quantify the geometry of the random grain structure. Here we concentrate on quantifications of grain size, and neglect a discussion of grain shape. Shape, while important to the correct modelling of polycrystalline microstructures, proves very difficult to quantify in a meaningful statistical way.

Grains are three dimensional volumes which are differentiated from neighboring grains by a change in crystallographic orientation at the grain boundaries. The only true measure of grain size is therefore the grain volume.

Determination of grain volume is unfortunately highly difficult experimentally. Some results have been obtained using serial sectioning methods [28] or by the chemical decomposition of a polycrystal into its constituent grains, which can then have their volumes measured. New three dimensional imaging techniques hold the promise of more efficient direct measurement of grain volumes.

The difficulty in obtaining measurements of grain volumes means that most often measurements of grain size are performed on two dimensional sections of three dimensional microstructures. Measurements of grain area can be obtained exactly by measuring the grain area directly, or approximately by determining the size of the largest possible inscribed circle for a given grain section.

For one dimensional measurements, by far the most common, the typical approach is to use a *line-intercept* method. In this procedure a series of randomly oriented lines is superimposed on the two dimensional polycrystal section. The lines are divided at intersections with grain boundaries, and statistics of the grain size are calculated from the lengths of the line segments so determined. The line-intercept method thus provides an estimate of the probability density of the one dimensional grain size. The remaining question is how this statistic relates to the statistics of the actual grain volume. Experimental investigations [28] provide two significant results.

1. The grain size distribution is well fit by a gamma distribution in 1, 2, or 3 dimensions.
2. The average line intercept length $\bar{L}$, the average grain area $\bar{A}$ and the average grain volume $\bar{V}$ are related by

$$\bar{L} = C_1 \bar{A}^{1/2} = C_2 \bar{V}^{1/3} \tag{1.24}$$

where the constants C_1 and C_2 are close to unity.

These results show that an experimental quantification of the grain size distribution in one dimension provides a complete description of the actual grain size distribution of the microstructure.

2. Probabilistic models for polycrystals

In the first section statistical characterizations of random microstructures were discussed. In this section and the next we address procedures for modelling random heterogeneous polycrystals and composite materials. This section addresses polycrystals and the next composites. In the final section such materials will be used in an application to the analysis of the fracture of random microstructures.

We begin with some definitions of terms and features relevant to the modelling of polycrystalline microstructures, and then present, in turn, probabilistic models for the grain geometry and crystallographic orientation of polycrystals. We will close with a section addressing the generation of samples from the probabilistic models which match target statistics determined from experimental measurements. Other approaches to the probabilistic modelling of polycrystals have been developed by other researchers [36, 37, 3, 38, 13, 20, 8, 12, 39, 27].

2.1. Definitions and features

In seeking to develop models for random microstructures which are useful in the analysis of small scale fracture phenomena, the first question which must be answered is which features to include in any such model. Uncertainty in fracture phenomena in polycrystalline materials becomes particularly important when the length scale of the fracture is on the order of the grain size of the material microstructure. There are important material features at smaller scales which may dramatically effect the fracture behavior, such as dislocations and systems of dislocations, but here our attention is restricted to what might be called the *grain scale*. The most obvious feature of the grain scale microstructure is the grain geometry itself, which can be described by the network of grain boundaries which divides the material domain into individual grains. Also important will be the locally heterogeneous material properties of the microstructure. These material properties can be derived from the local *crystallographic orientation*, to be defined shortly. A description of the grain geometry and the crystallographic orientation therefore provides suitably detailed, if not complete, information about the grain scale microstructure for application to small scale fracture analysis.

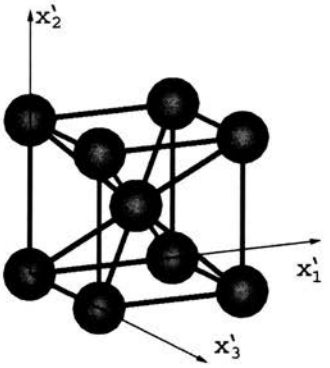

FIGURE 3. Definition of crystal coordinate system.

The atoms in a crystalline solid are arranged on a regular grid, or lattice. There are a variety of different lattice configurations possible in real materials, such as body centered cubic, face centered cubic, and hexagonal close packed, but in each case the regular arrangement of atoms can be used to establish an orthogonal coordinate system (x_1', x_2', x_3'), called the *crystal coordinate system* (Fig. 3). The *crystallographic orientation* gives the transformation from some reference coordinate system (x_1, x_2, x_3) to the crystal coordinate system.

There are numerous representations of the orientation, many of which are defined in detail in the book by Randle [32]. We will make use of three of these representations;

1. The *rotation tensor* representation, in which the transformation from reference to crystal coordinates is given by a second order tensor $\mathbf{R}$ so that a vector $\mathbf{x}$ is transformed to crystal coordinates by $\mathbf{x}' = \mathbf{R}\mathbf{x}$.
2. The *Euler angle* representation describes the transformation by a series of three rotations given by the angles ϕ_1, Φ, ϕ_2.
3. The *axis/angle* representation gives the transformation by a single rotation θ about a specified axis $[UVW]$.

The Euler angle representation has the advantage that it is easily adaptable to the random field description of microstructure which we have previously introduced. We will, as before, alter the notation slightly so that the orientation field is denoted by $\mathbf{Y} = [\Psi_1, \Psi_2, \Psi_3]^T$ where $\Psi_1 = \phi_1$, $\Psi_2 = \Phi$, $\Psi_3 = \phi_2$, and the capital letters are used to denote that the Euler angles are random.

The axis/angle representation has the advantage that the angle θ can be thought of as a low order, scalar descriptor of the amount of rotation needed to get from the reference to crystal coordinate systems. This feature of the axis/angle representation makes it particularly useful when referring to the *misorientation.*

Whereas the orientation gives the transformation from a reference to a crystal coordinate system, the misorientation gives the transformation from one crystal coordinate system to another. With respect to the microstructure, therefore, the misorientation quantifies the difference in orientation between two points in the polycrystal. Reference to misorientation is most commonly made with respect to the orientation discontinuity which arises at *grain boundaries.* Orientation typically undergoes only very small fluctuations within grains, and larger, discontinuous variation at grain boundaries. Each grain boundary therefore has associated with it a specific misorienta-

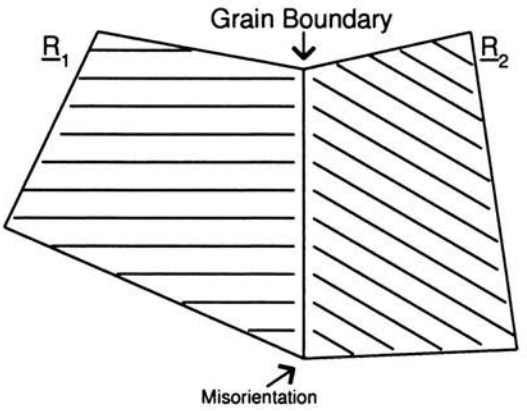

FIGURE 4. Schematic illustration of misorientation at grain boundary.

tion (Fig. 4) which is calculated by

$$\mathbf{M} = \mathbf{R}_2\mathbf{R}_1^{-1} \tag{2.1}$$

where $\mathbf{R}_1$, $\mathbf{R}_2$ are the rotation tensor representations of the orientation of grains 1 and 2 and the misorientation gives the rotation from $\mathbf{R}_1$ to $\mathbf{R}_2$. From the rotation tensor representation $\mathbf{M}$ of the misorientation, the Euler angle or axis/angle representations can be derived. When the axis/angle form is used to represent a misorientation, the angle θ is called the *angle of misorientation* and can be thought of as a scalar representation of the misorientation between two grains. That is, two grains which have a misorientation with large θ are said to be highly misoriented.

2.2. Grain geometry

The probabilistic model selected for the grain geometry is the Poisson-Voronoi tessellation. The model is described here in two dimensions, and the examples are also given in two dimensions, but are easily extended to model three dimensional microstructures. More detailed discussion of the properties of random tessellations can be found in the book by Stoyan [34].

Begin by defining a set of nuclei for the grains, denoted by $\{\mathbf{n}_i\}$, with $\mathbf{n}_i \in S$ where S is the microstructure domain. The grains, modelled by the Voronoi tessellation constructed on these nuclei, are defined by

$$P_i = \{\mathbf{x} \in S : \| \mathbf{x} - \mathbf{n}_i \| < \| \mathbf{x} - \mathbf{n}_j \|, j \neq i\} \tag{2.2}$$

where P_i is the polygon, or grain, associated with nucleus n_i. The geometric meaning of this definition is that each polygon contains all the points

in S which are closer to its associated nucleus than any other. The physical assumption associated with using this tessellation to model polycrystalline materials is that the grains nucleate simultaneously and grow homogeneously and isotropically.

The randomness in the grain geometry is introduced by modelling the nuclei as a *Poisson point field* $N(S')$ where $S' \subset S$. A Poisson point field is governed by the intensity function $\lambda(\mathbf{x})$ which describes the average number of points per unit area at location $\mathbf{x} \in S$. Certain properties of the point field are defined by the intensity function, for example, the average number of points in realizations of the field on the domain S. This value is given by

$$\bar{N} = \int_S \lambda(\mathbf{x}) d\mathbf{x} \tag{2.3}$$

and is the mean value of the random variable $N(S)$, the number of points in S, which is Poisson distributed with probability mass function

$$p(n, \bar{N}) = \frac{e^{-\bar{N}} \bar{N}^n}{n!} \tag{2.4}$$

which gives the probability of having n points in S.

The intensity function has so far been defined as a function of position, corresponding to the general assumption that the Poisson point field is non-stationary, or inhomogeneous, and that the average grain size varies spatially. Assuming homogeneity of the intensity function renders the intensity a constant so that $\lambda(\mathbf{x}) = \lambda$.

Example 6. Figure 5 shows two independent realizations of a homogeneous Poisson point field on the unit square with $\lambda = 100$. In the left realization the total number of nuclei is $n = 101$, and in the right the total number is $n = 83$.

Example 7. Figure 6 shows two independent realizations of the inhomogeneous Poisson point field with intensity function $\lambda(\mathbf{x}) = 1000 \parallel \mathbf{x} \parallel^3$ on the unit square. The expected number of points in the realizations is 629, and the samples shown have 631 and 600 points respectively.

Given this model for the grain geometry we are left to determine how to calibrate the intensity function to achieve a grain structure with the desired average grain sizes. Intuition and dimensional arguments suggest that $\lambda \propto \bar{A}^{-1}$ for the case of a homogeneous microstructure, but it is left to be determined what the constant of proportionality is, and whether a similar relationship holds for polycrystals with inhomogeneous average grain size.

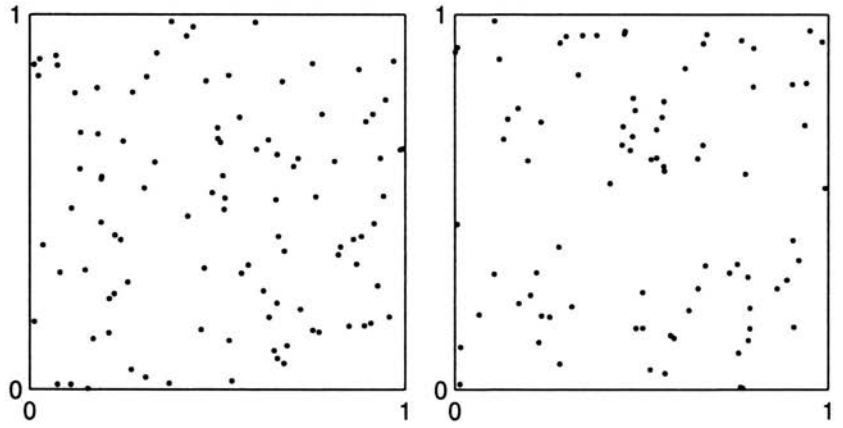

FIGURE 5. Independent samples of a homogeneous Poisson point process.

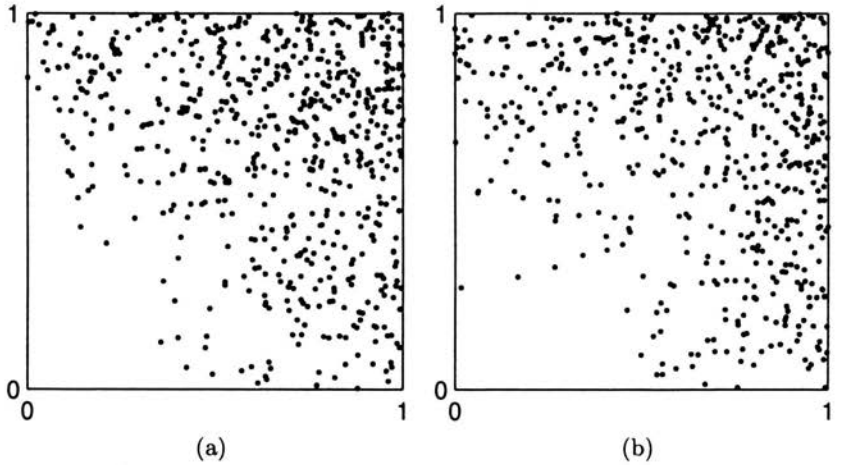

FIGURE 6. Independent samples of an inhomogeneous Poisson point process.

Before addressing these questions, we state the simplest case of calibration of the Poisson point field for the grain nuclei. Suppose that there is a sample two dimensional microstructure, occupying a domain S which has been found experimentally to consist of n grains. Provided that the assumption of stationarity is reasonable, the intensity can be calibrated as

$$\lambda(\mathbf{x}) = \lambda = \frac{n}{\int\limits_S dA}. \tag{2.5}$$

This calibration assures that, on average, sample realizations of the Poisson point field will have $\bar{N} = n$ nuclei.

For polycrystalline microstructures with inhomogeneous average grain size, calibration by Eq. (2.5) cannot provide adequate information since the calibrated intensity function must be a function of position. A moving window technique can be applied, and is often the only practical method of estimating the local average grain size. Such a technique has the disadvantage, however, of providing an estimate of the average grain size which depends upon the chosen window size.

For this reason, we here introduce some results regarding the relationship between the intensity function $\lambda(\mathbf{x})$ and the ensemble average grain size at $\mathbf{x}$, denoted by $\langle A(\mathbf{x})\rangle$. The ensemble average grain size is determined by taking a fixed point $\mathbf{x}$ and, for a collection of q microstructure realizations, computing

$$\langle A(\mathbf{x})\rangle = \frac{1}{q}\sum_{i=1}^{q} A(P_i(\mathbf{x})) \tag{2.6}$$

where $A(P_q(\mathbf{x}))$ is the area of the grain containing $\mathbf{x}$ in realization q.

We begin with the exact solution to a one dimensional, homogeneous average grain size, version of the calibration problem. Figure 7 shows the one dimensional version of the random grain geometry with nuclei and grain boundaries indicated. The problem is to determine $E[L(x)]$ given the specified intensity λ. This is in fact the inverse of the calibration problem, but solution provides the same information.

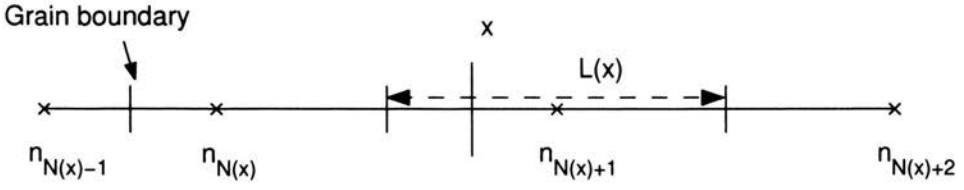

FIGURE 7. Arrangement of nuclei and grains in a one dimensional Voronoi tessellation.

The result is obtained by conditioning on the number of nuclei to the right and left of x [5, 4], and is

$$\langle L(x)\rangle = \langle L\rangle = \frac{3}{2\lambda} \tag{2.7}$$

provided x is far away from the boundaries. There is a boundary effect altering the proportionality constant within about five average grain sizes of the

microstructure boundaries. From this result we conclude that the ensemble average grain size is larger by one half than the inverse of the intensity.

For inhomogeneous intensity the result is found, by Monte Carlo simulation, to be

$$\langle L(x) \rangle = \frac{3}{2\lambda(x)}. \tag{2.8}$$

Figure 8 demonstrates this result by showing the results of a Monte Carlo simulation in which sample microstructures were realized after calibrating the intensity function according to Eq. (2.8). The relationship is confirmed, again with a boundary effect evident.

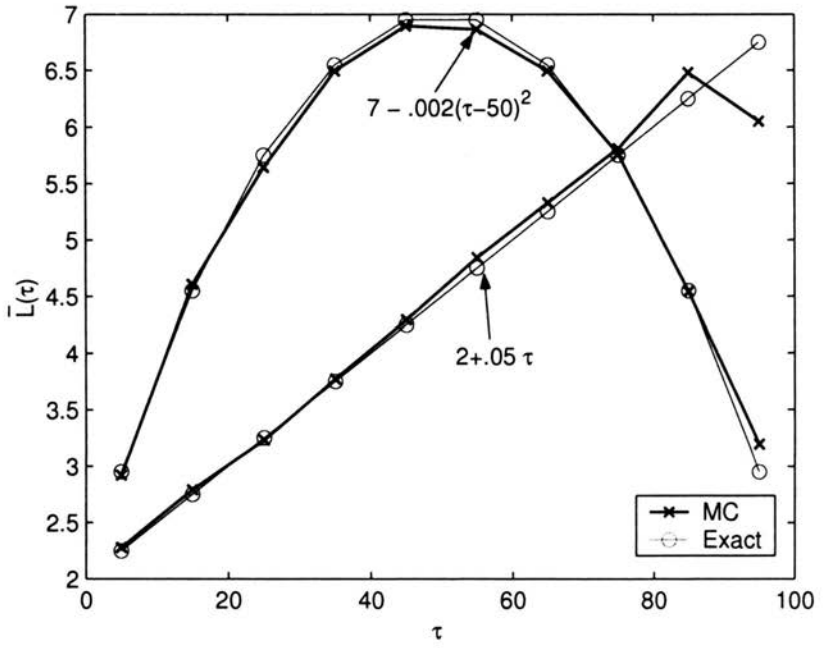

FIGURE 8. Results of Monte Carlo simulation showing relationship between average grain size and nucleus intensity for one dimensional microstructure.

Monte Carlo simulations indicate that the inverse proportionality holds in two and three dimensions so that

$$\langle A(\mathbf{x}) \rangle = 1.28\lambda(\mathbf{x}) \tag{2.9}$$

and

$$\langle V(\mathbf{x}) \rangle = 1.40\lambda(\mathbf{x}). \tag{2.10}$$

2.3. Crystallographic orientation

In developing a random field model for the crystallographic orientation the first decision is what degree of detail is required in the model. Recall that we define the random field to be

$$\mathbf{Y}(\mathbf{x}) = [\Psi_1, \Psi_2, \Psi_3]^T \tag{2.11}$$

and that we have a choice in developing a method for characterizing this field. One option would be to estimate as many of the finite dimensional distributions as possible. Here we will instead adopt the second moment characterization augmented by the marginal distributions of the random field components. The calibration functions are therefore $F_i(\psi, \mathbf{x})$ and $\boldsymbol{\rho}(\mathbf{x}, \mathbf{z})$, the marginal distributions and scaled covariance function respectively.

The orientation random field has samples which are highly non-Gaussian and, in a polycrystalline material, discontinuous at the grain boundaries. Fields which have discontinuities with random geometry are very difficult to simulate. A simplifying assumption is therefore made by which $\mathbf{Y}(\mathbf{x})$ is assumed to be constant within each grain. The orientation field can be represented completely by a combination of the grain geometry and a set of random vectors $\mathbf{Y}_i$, $i = 1, \ldots, n$ where n is the number of grains in the realization and $\mathbf{Y}_i$ gives the orientation in grain P_i. As will be seen in the discussion of sample generation, this simplification results in straightforward realization of the orientation field.

The above assumption, which implies that the orientation field exists conditional upon the grain geometry, results in a direct connection between the statistics of the orientation field and the grain geometry, particularly between the scaled covariance function $\boldsymbol{\rho}(\mathbf{x}, \mathbf{z})$ and the nucleus intensity $\lambda(\mathbf{x})$.

Suppose that there is an underlying scaled covariance function which is stationary and isotropic and which depends upon separation distance normalized by the average grain diameter. We illustrate the concept using a scalar random field rather than the actual orientation field for simplicity, but the approach is equally applicable to vector random fields. Let the underlying stationary, isotropic scaled covariance function be denoted by $\tilde{\rho}(\tilde{d})$ where $\tilde{d} = d/\sqrt{\bar{A}}$ is the non-dimensional separation distance and it is assumed that $\bar{A} = 1$, that is, the underlying homogeneous microstructure has grains with average area equal to unity. The effective distance for two points in the sample microstructure with inhomogeneous average grain size is given by

$$\tilde{d}(\mathbf{x}, \mathbf{z}) = \int_{l_{\mathbf{xz}}} \sqrt{\lambda(\mathbf{u})/C}\, ds \tag{2.12}$$

where $l_{\mathbf{xz}}$ is the line segment connecting points $\mathbf{x}$ and $\mathbf{z}$ and C is a constant which is unity if $\bar{A}$ is intended as spatially averaged quantity and 1.28 the averaging is made in the ensemble sense. The non-stationary and anisotropic scaled covariance function of $Y(\mathbf{x})$ is then given by

$$\rho(\mathbf{x}, \mathbf{z}) = \tilde{\rho}(\tilde{d}(\mathbf{x}, \mathbf{z})). \tag{2.13}$$

Example 8. Let S be a polycrystal with grain intensity given by

$$\lambda(\mathbf{x}) = \frac{1.3}{(3.5|x_1| + 900)\,\mu\text{m}^2} \tag{2.14}$$

with $S = [-2000, 2000]^2$. Assume $C = 1$ for the constant of Eq. (2.12). Figure 9 shows a realization of the grain geometry. Grains are smaller near $x_1 = 0\,\mu$m. All dimensions are given in microns unless otherwise noted.

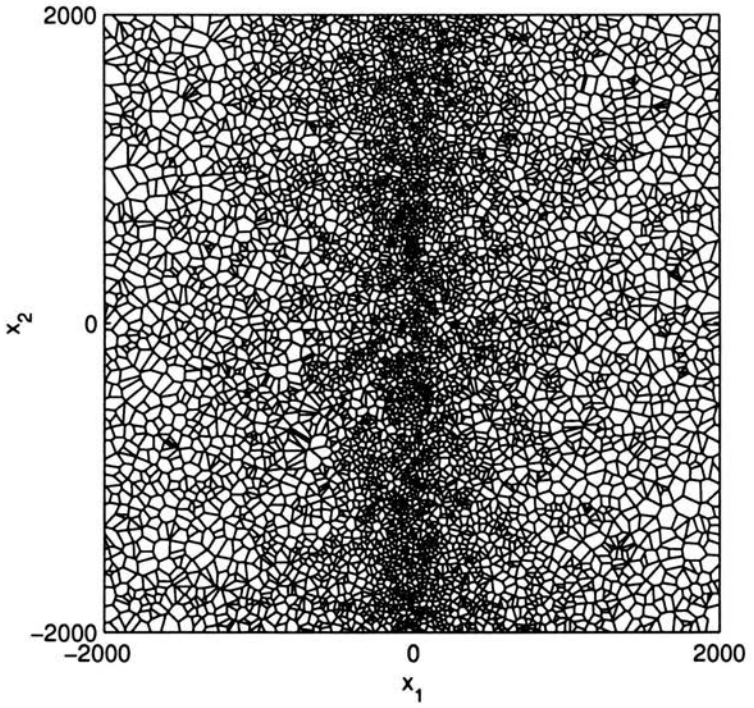

FIGURE 9. Grain geometry realization for intensity function of Eq. (2.14).

In this example a scalar correlation function is used. Extension to multivariate fields, as required by the orientation, is straightforward. The underlying spatially invariant correlation function is $\tilde{\rho}(d) = \exp(-\tilde{d})$ so that

$\rho(\mathbf{x},\mathbf{z}) = \exp(-\tilde{d}(\mathbf{x},\mathbf{z}))$ with $\tilde{d}(\mathbf{x},\mathbf{z})$ defined by Eq. (2.12). The normalization of d by the average grain size is not denoted explicitly here since the average grain size is assumed to be unity.

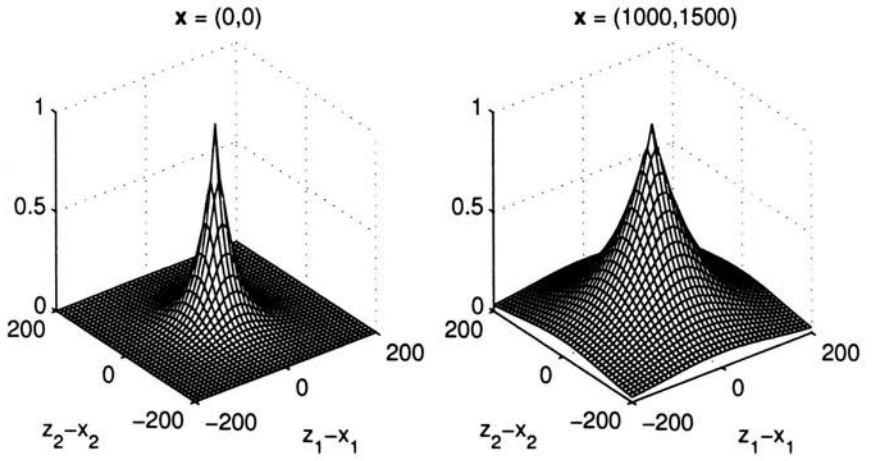

FIGURE 10. Correlation function $\tilde{\rho}(\mathbf{x},\mathbf{z})$ at $\mathbf{x} = (0,0)$ and $\mathbf{x} = (1000, 1500)$.

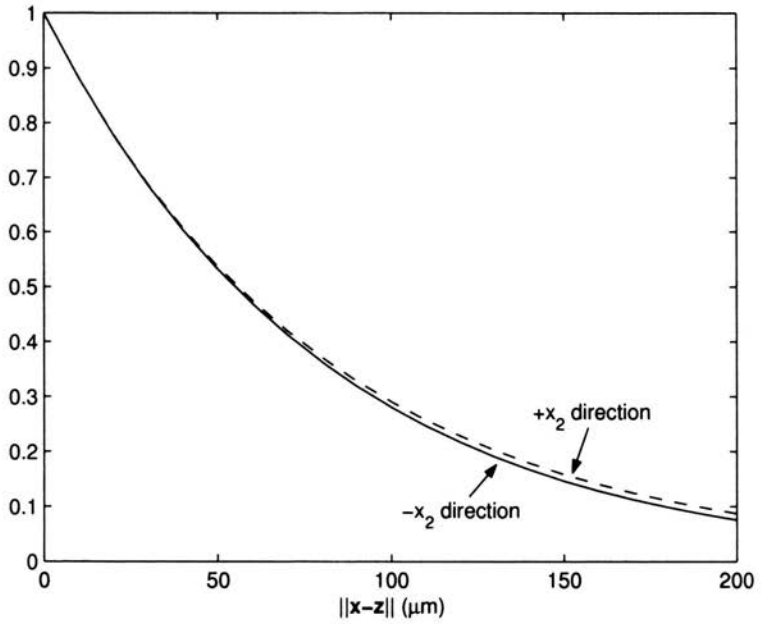

FIGURE 11. Anisotropy of correlation function $\tilde{\rho}(\mathbf{x},\mathbf{z})$ at $x = (1000, 1500)$.

The correlation function $\rho(\mathbf{x}, \mathbf{z})$ of the inhomogeneous microstructure is shown in Fig. 10 at the points $\mathbf{x} = (0, 0)$ and $\mathbf{x} = (1000, 1500)$. The correlation decays more gradually at $\mathbf{x} = (1000, 1500)$, where the average grain size is larger. Anisotropy of the correlation function is illustrated in Fig. 11, which shows more persistent correlation in the direction of increasing x_1. This corresponds to the direction in which the grain intensity decreases.

Example 9. We now present some calibration statistics taken from an actual experimental observation of an aluminum 2024 polycrystal. The Euler angles, obtained by electron backscatter diffraction [26, 1], are shown in Fig. 12. The total experimental sample consists of 14 000 data points on a sample which is $540\,\mu\text{m} \times 540\,\mu\text{m}$ and contains 120 grains. Assuming homogeneity of the grain geometry the average grain size is $2430\,\mu\text{m}^2$ and the corresponding intensity is 4×10^{-4}. The grain geometry indicates that the stationary and isotropic assumptions may apply, and, due to the lack of contradictory evidence, these assumptions are made. The marginal histograms

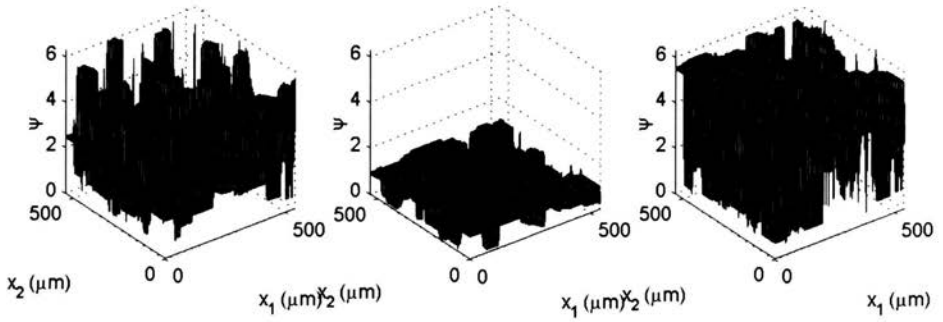

FIGURE 12. Sample Euler angle measurements.

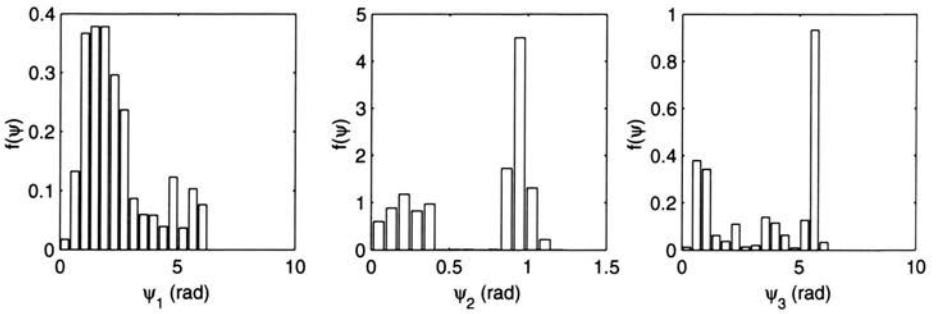

FIGURE 13. Sample Euler angle measurements.

are estimated for the three Euler angles (Fig. 13), and illustrate the highly non-Gaussian nature of the data.

The scaled auto- and cross-covariance functions have been estimated and are shown in Fig. 14. They exhibit an exponential decay $a\exp(-bd)$ which is best fit by the functions given in Table 1.

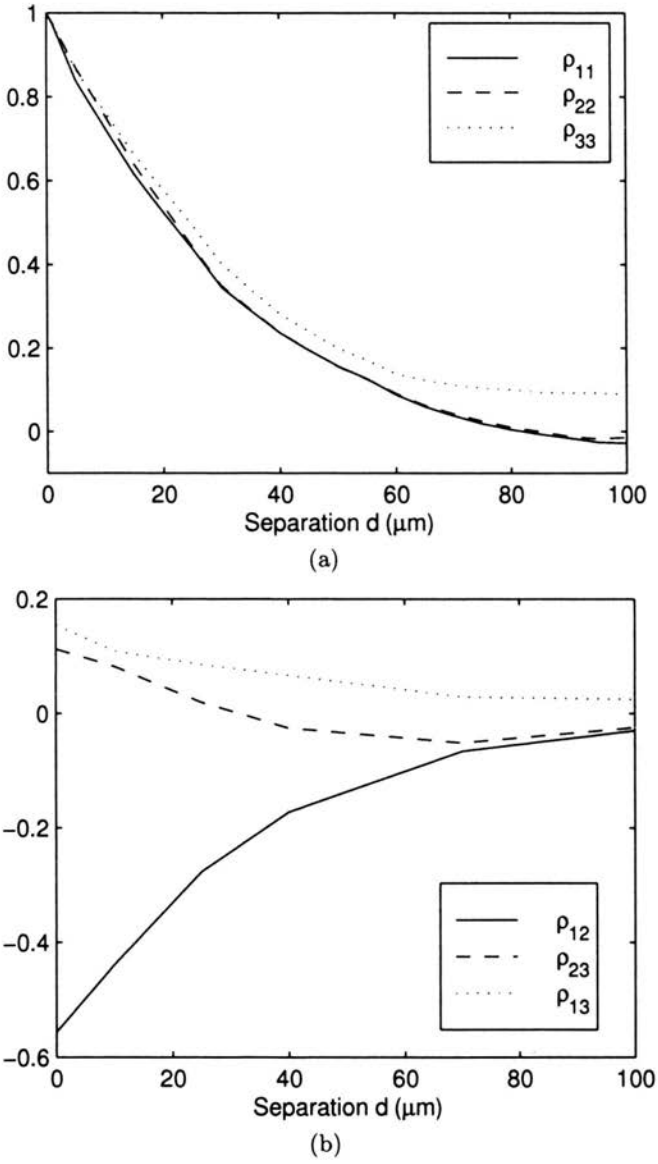

FIGURE 14. Scaled covariance function of experimentally obtained Euler angles.

TABLE 1. Parameters of the orientation scaled covariance functions as estimated from data.

	a_{ij}	b_{ij}
$\rho_{11}(d)$	1.0	0.036
$\rho_{22}(d)$	1.0	0.035
$\rho_{33}(d)$	1.0	0.030
$\rho_{12}(d)$	-0.57	0.030
$\rho_{13}(d)$	0.14	0.021
$\rho_{23}(d)$	0.13	0.012

2.4. Sample generation

The generation of sample microstructures takes place in two stages:

1. the generation of a sample grain geometry and
2. the generation of a sample of the orientation field conditional upon the grain geometry realization.

If a sample microstructure is to be generated in a domain S with a specified nucleus intensity function $\lambda(\mathbf{x})$, the first step is to generate a realization of the nuclei $\mathbf{n}_i$. This is accomplished by the following procedure:

1. Calculate $\bar{N} = \int_S \lambda(\mathbf{x})d\mathbf{x}$, the expected number of grains in the microstructure.
2. Generate a realization n of the Poisson random variable $N \sim poiss(\bar{N})$.
3. Determine $\lambda_{\max} = \max\{\lambda(\mathbf{x}) : \mathbf{x} \in S\}$.
4. Generate a point $\mathbf{n}^*$ which has coordinates uniformly distributed on S.
5. Retain $\mathbf{n}^*$ as one of the sample nuclei with probability $\lambda(\mathbf{n}^*)/\lambda_{\max}$.
6. Repeat steps 4 and 5 until n points have been retained as nuclei.

Once the set of nuclei has been generated, it is straightforward to calculate the geometry of the grains $\{P_i\}$ using one of several readily algorithms, for example the `qhull` algorithm implemented in `MATLAB` [31].

By assuming that the orientation is constant within each grain, the orientation field can be specified by the set of random vectors $\{\mathbf{Y}_i\}$. Define the vectors to give the orientation at the centroid $\mathbf{c}_i$ of each grain P_i.

We then arrange the orientation variables into a single large random vector $\hat{\mathbf{Y}}$ which, combined with the already realized grain geometry, provides a complete description of the microstructure random field. The vector $\hat{\mathbf{Y}}$ is defined by

$$\hat{\mathbf{Y}} = [\mathbf{Y}_1, \mathbf{Y}_2, \mathbf{Y}_3]^T \tag{2.15}$$

where $\mathbf{Y}_k$ is the $n-dimensional$ vector containing the kth Euler angle of the n grains in the microstructure. This random vector is characterized in second moment by the vectors $\hat{\boldsymbol{\mu}} = [\boldsymbol{\mu}_1, \boldsymbol{\mu}_2, \boldsymbol{\mu}_3]^T$ and $\hat{\boldsymbol{\sigma}} = [\boldsymbol{\sigma}_1, \boldsymbol{\sigma}_2, \boldsymbol{\sigma}_3]^T$ representing the mean and standard deviation of the orientation in each of the grains, as well as the $3n \times 3n$ scaled covariance matrix

$$\hat{\boldsymbol{\rho}} = \begin{bmatrix} \boldsymbol{\rho}_{11} & \boldsymbol{\rho}_{12} & \boldsymbol{\rho}_{13} \\ \boldsymbol{\rho}_{21} & \boldsymbol{\rho}_{22} & \boldsymbol{\rho}_{23} \\ \boldsymbol{\rho}_{31} & \boldsymbol{\rho}_{32} & \boldsymbol{\rho}_{33} \end{bmatrix} \tag{2.16}$$

where

$$[\boldsymbol{\rho}_{ij}]_{kl} = \rho_{ij}(\mathbf{c}_k, \mathbf{c}_l). \tag{2.17}$$

The problem of generation of the sample orientation field is now reduced to the problem of generating a sample of the non-Gaussian random vector $\hat{\mathbf{Y}}$ which matches the second moment properties of the orientation field and the marginal distributions. This is accomplished by use of *translation models*, in which the non-Gaussian random vector is created as a transformation of a Gaussian random vector, which is straightforward to simulate [18, 17, 19]. The only complication is that in transforming from the Gaussian to non-Gaussian state, the covariance function of the random vector is distorted. The scaled covariance $\hat{\boldsymbol{\rho}}_g$ of the underlying Gaussian random vector must therefore be determined before simulation can proceed. This calibration is carried out using

$$\mu_i \mu_j + \sigma_i \sigma_j [\hat{\boldsymbol{\rho}}_{ij}]_{kl} = \int_{-\infty}^{\infty} \int_{-\infty}^{\infty} g_i(u) g_j(v) \phi(u, v; [\hat{\boldsymbol{\rho}}_{g,ij}]_{kl}) \, du \, dv \tag{2.18}$$

where $\phi(\cdot, \cdot; \rho)$ is the bivariate Gaussian density function with correlation coefficient ρ, and $g_i(\cdot)$ is defined by

$$g_i(\cdot) = F_i^{-1} \circ \Phi(\cdot) \tag{2.19}$$

where F_i^{-1} is the inverse cdf of Euler angle Ψ_i, and $\Phi(\cdot)$ is the standard Gaussian cdf. Equation (2.18) gives the non-Gaussian scaled covariance in terms of the Gaussian scaled covariance. Since the modeler usually has as a target the non-Gaussian covariance, the equation must be solved inversely to calibrate the Gaussian scaled covariance.

Once the entries of $\hat{\boldsymbol{\rho}}_g$ have been calculated, the sample generation procedure is as follows. First, a standard normal Gaussian random vector, of dimension $3n \times 3n$ is generated with independent components,

$$\mathbf{Z} \sim N(\mathbf{0}, \mathbf{I}) \tag{2.20}$$

where $\mathbf{I}$ is the identity matrix. Next, $\mathbf{Z}$ has the appropriate correlation structure introduced by the operation

$$\mathbf{V} = \boldsymbol{\beta}\mathbf{Z} \tag{2.21}$$

where $\boldsymbol{\beta}$ is the Cholesky decomposition of $\hat{\boldsymbol{\rho}}_g$. Finally, the realization of $\hat{\mathbf{Y}}$ is created by

$$\hat{Y}_i = \begin{cases} g_1(V_i), & 1 \leq i \leq n, \\ g_2(V_i), & n < i \leq 2n, \\ g_3(V_i), & 2n \leq i \leq 3n. \end{cases} \tag{2.22}$$

3. Probabilistic models for composites

The previous section contained a description of a two part probabilistic model for polycrystalline microstructures which included the grain geometry and crystallographic orientation. In this section the topic of discussion will be composite materials, and appropriate probabilistic models for them.

3.1. Scope and definitions

The term "composite materials" encompasses a set of materials with a broad range of material microstructures, some random and some deterministic. Examples include traditional materials like concrete and even wood, as well as more modern materials such as fiber reinforced polymers, and carbon fiber composites. The microstructures of these materials differ significantly from one another. A concrete microstructure, for example, consists of arbitrarily shaped aggregate particles suspended in a cement paste matrix. In a fiber reinforced polymer on the other hand straight or curved fibers are embedded in a polymer matrix. The fibers can be deterministically or randomly oriented.

There is an abundance of models available for representing composite microstructures which consist of fibers embedded in a matrix, most of which are described in [35]. Many of these models seek to represent two dimensional cross sections. One feature of such materials is that the geometry of the reinforcement phase is generally deterministic, for example, a cross section of a fiber reinforced composite can be modelled by a Poisson point process giving the location of disks representing the fibers in the matrix.

In this section we do not focus on this type of material, for which models are already well developed, but rather on a type of composite in which the geometry of the phases is entirely random. The material consists of multiple

phases, and the local volume fraction of each is denoted by ϕ_i for phase i, which we recall is the 1-point probability function of the phase. The microstructure of the n-phase material can be specified by the set of $n-1$ indicator functions $I_i(\mathbf{x})$, $i = 1, \ldots, n-1$. Examples of such multi-phase materials include concrete, which can be modelled as a two phase material consisting of the aggregate and the cement paste, or as a three phase material with the inclusion of a transition zone between the aggregate and matrix, porous materials such as sandstone which consists of two phases, the solid phase and the void phase, and functionally graded composites, which have the additional complication of having non-stationary statistics.

In this presentation two methods of generating realizations of such multi-phase materials are presented and examples given. In both approaches, the sample generation technique relies upon discretization of the microstructure domain into pixels. The sample generation procedure then consists of assigning the appropriate phase to each of the pixels in order to recreate a realization of the microstructure. The first method presented here has been developed by Deodatis and Koutsourelakis [14]. It utilizes level crossings of a Gaussian random process to determine the location of the phases of a two phase material, and is given in outline form here. For details, reference should be made to the original papers of the originators. The second approach uses translation models to realize the non-Gaussian random field of the indicator functions representing the microstructure.

3.2. Multiphase materials I

As described previously, a random two-phase material can be described by the indicator function for phase one, $I_1(\mathbf{x})$ which is unity if $\mathbf{x}$ is in phase one and zero otherwise. Since only one indicator function is necessary to describe the two phase material, the subscript will be dropped from this point on. This indicator function forms a binary random field which has samples with the discrete probability mass function

$$p(u, \mathbf{x}) = \phi_1(\mathbf{x})\delta(u) + (1 - \phi_1(\mathbf{x}))\delta(u-1) \tag{3.1}$$

where $\phi_1(\mathbf{x}) = E[I(\mathbf{x})]$ is the local volume fraction of the first phase and $\delta(\cdot)$ is the Dirac delta function. The method described here will produce microstructure realizations which are stationary and which can match a target volume fraction and second order correlation function, equivalent to the 2-point probability function defined by

$$r(d) = E[I(\mathbf{x})I(\mathbf{x} + d\mathbf{e})] = P[\text{both points } \mathbf{x} \text{ and } \mathbf{x} + d\mathbf{e} \text{ are in phase 1}] \tag{3.2}$$

where $\mathbf{e}$ is a unit vector with arbitrary direction and d is a scalar separation distance.

The simulation scheme is first described for a one dimensional microstructure, and then the extension to two dimensions is presented. The one dimensional microstructure domain S is divided into n pixels with centers located at the points $\{x_i\}$ and length Δx. The first step in realization of the microstructure is the generation of a stationary series of Gaussian random variables $\{Z_i\}$ which have zero mean and unit variance and a correlation function denoted by $\rho(\| i - j \|) = E[Z_i Z_j]$. This series of random variables can also be thought of as denoting the values $\{Z(x_i)\}$ of a Gaussian random process $Z(x)$ with correlation function $\rho(d)$. A sequence of stationary binary random variables is generated from this sequence of Gaussian variables by

$$Y_i = \begin{cases} 1, & Z_{i-1} Z_i < 0 \\ 0, & \text{otherwise.} \end{cases} \tag{3.3}$$

which has correlation function $r(\| i - j \|) = E[Y_i Y_j]$. From this series the random process describing the random microstructure is reconstructed by

$$Y(x) = Y_i,\ x \in [x_i - \Delta x, x_i + \Delta_x) \tag{3.4}$$

and has correlation function $r(d)$. The microstructure random field takes a value of 1 in intervals where there is an odd number of zero crossing of the Gaussian random process $Z(x)$.

The key procedure in generating realizations using this method which match a specified target correlation function $r(d)$ is to identify the appropriate correlation function $\rho(d)$ for the underlying Gaussian process. Deodatis and Koutsourelakis [14] have derived expressions for determining $r(0)$, $r(\Delta x)$ in terms of $\rho(0)$, $\rho(\Delta x), \rho(2\Delta x)$. These expressions are

$$\begin{aligned} r(0) &= \phi_1 = \frac{1}{\pi} \arccos(\rho(\Delta x)), \\ r(\Delta x) &= \frac{1}{4} + \frac{1}{2\pi} \left(\arcsin(\rho(2\Delta x) - 2 \arcsin(\rho(\Delta x))) \right). \end{aligned} \tag{3.5}$$

The volume fraction is determined by the correlation coefficient of sequential elements of the Gaussian series $\{Z_i\}$ and the correlation of sequential elements of the microstructure series $\{Y_i\}$, $r(\Delta x)$ is determined by the Gaussian correlations $\rho(\Delta x)$ and $\rho(2\Delta x)$. In general, exact expressions have not been developed for calculating the values $r(m\Delta x)$ for $m > 1$ from the correlations of the Gaussian series, though these values can be obtained by numerical calculation of fourth order integrals.

Example 10. Figure 15 shows three pairs of Gaussian and microstructure correlation functions. The corresponding microstructural samples (Fig. 16) show the ability of the method to reproduce materials with varying degrees of clustering.

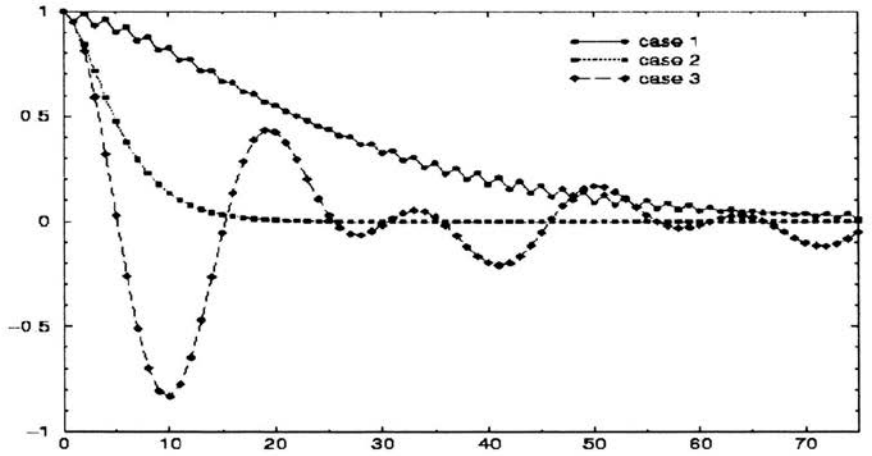

(a) Gaussian correlation functions

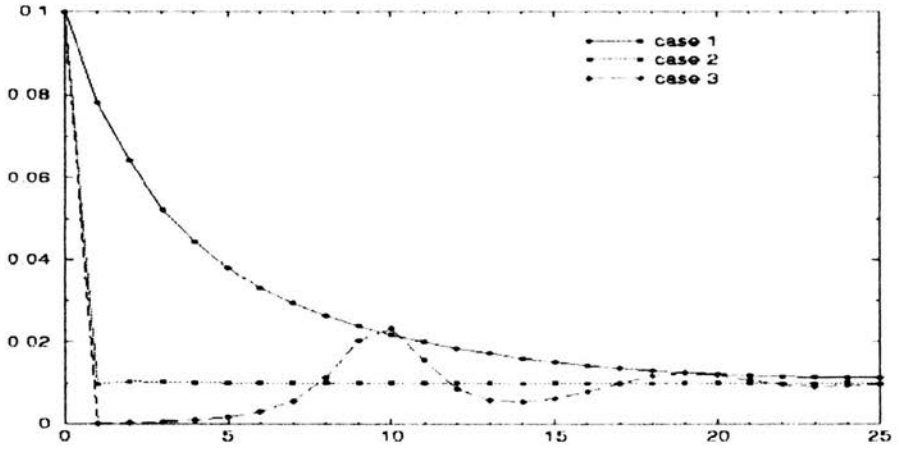

(b) Microstructure correlation functions

FIGURE 15. Gaussian and binary correlation functions for two phase medium. (Figure courtesy Deodatis and Koutsourelakis [14]).

Since exact expressions are not available for the relationship of the complete Gaussian and microstructure correlation functions, a numerical optimization scheme is adopted to determine the appropriate Gaussian correlation function for matching a desired microstructure correlation function. In

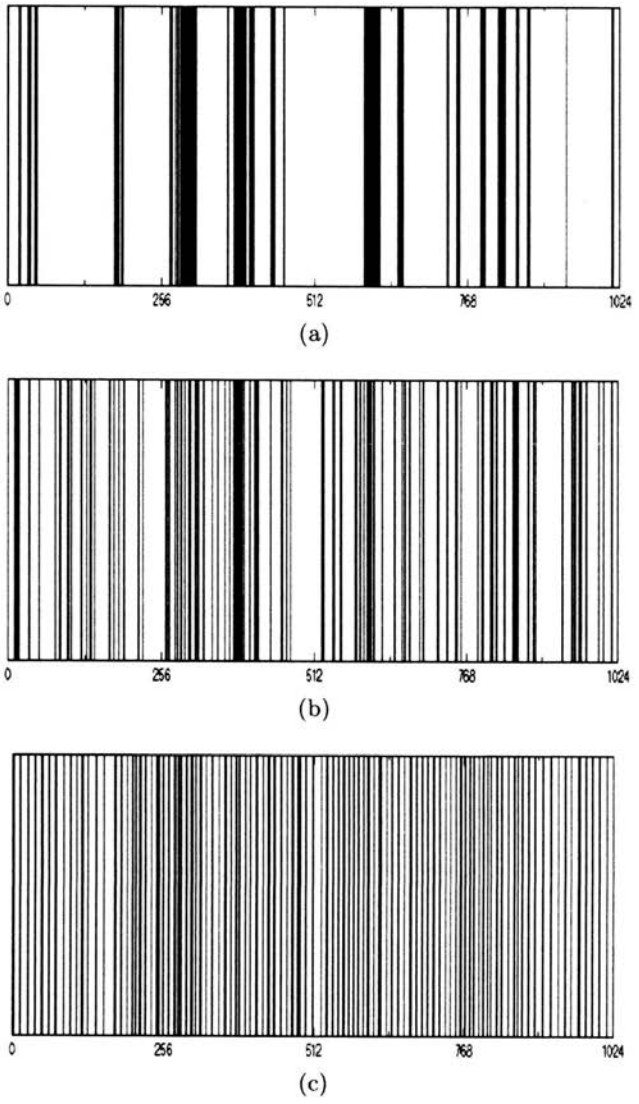

FIGURE 16. Sample microstructures generated from the correlations of Fig. 15. (Figure courtesy Deodatis and Koutsourelakis [14]).

describing this procedure in outline form we will make use of the random process notation for the underlying Gaussian $Z(x)$ and its correlation function $\rho(d)$, and the microstructure $Y(x)$ and its correlation function $r(d)$.

The optimization method makes use of the spectral density functions $s(\omega)$, and $s_g(\omega)$, which are the Fourier pairs of $r(d)$ and $\rho(d)$ respectively.

The procedure used to determine the appropriate Gaussian spectral density to match the target microstructure correlation is:

1. Postulate a Gaussian spectral density function $s_g(\omega)$ as an initial condition on the optimization procedure.
2. Compute the Gaussian correlation function $\rho(d)$ using

$$\rho(i\Delta x) = \frac{\pi}{N_f}\left(S_0 + 2\sum_{k=1}^{N_f-1} S_k \cos\left(ki\frac{\pi}{N_f}\right) + S_N\cos(i\pi)\right) \tag{3.6}$$

   where N_f is the number of frequencies at which the spectral density is evaluated, and S_k is the value of the spectral density at these locations.
3. Calculate numerically the corresponding microstructure correlation function $r(d)$.
4. Compare $r(d)$ to the target microstructure correlation function $r_{\text{target}}(d)$ using an error measure $\max\{|r(d) - r_{\text{target}}(d)|\}$
5. If the error is greater than the desired accuracy, make small perturbations to $s_g(\omega)$. There are many possible approaches to making these perturbations. At present, the authors of this method use random perturbations which, while not the most efficient approach, are very easy to implement.
6. Repeat steps 2-4.
7. If the new error is smaller than the previous error, accept the changes to $s_g(\omega)$. If not, reject the changes.
8. Repeat 6-8 until the desired accuracy is attained in the microstructure correlation function $r(d)$.

Once the spectral density/correlation function of the underlying Gaussian has been determined, the sample generation procedure consists simply of

1. Generate a sample $z(x)$ of $Z(x)$ using any of several available methods for sampling Gaussian processes (sampling theorem, spectral representation, etc.).
2. Calculate $\{z(m\Delta x)\}$ for all pixels of the microstructure.
3. Calculate $\{y(m\Delta x)\}$ and $y(x)$ using Eqs. (3.3) and (3.4).

The simulation method presented above for one dimensional microstructures has been extended to two dimensions by Deodatis and Koutsourelakis [14]. Figure 17 shows an example of the output of the two dimensional simulation method in which the volume fraction and correlation function of the Fontainebleau sandstone are matched. The appearance of the sample is quite realistic, though it is equally apparent that some further statistical information is required in order to better match the details of the shapes of the

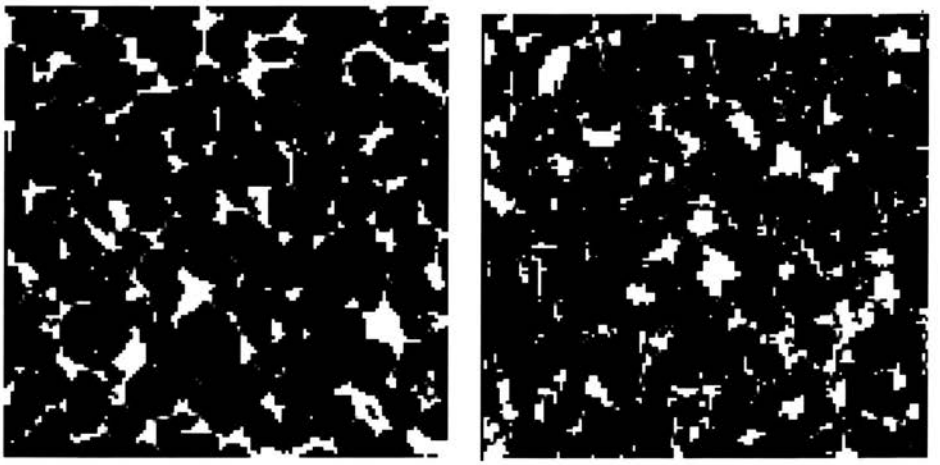

(a) Fontainebleau sandstone (b) Simulated Fontainebleau sandstone

FIGURE 17. Fontainebleau sandstone and simulated microstructure. (Figure courtesy Deodatis and Koutsourelakis [14]).

voids in the materials. It is possible that this may be accomplished through ongoing efforts to produce samples which match higher order moments of the microstructure random field.

3.3. Multiphase materials II

A method for generating realizations of n-phase composite material microstructures with prescribed correlation functions is described. The method relies on division of the material domain into pixels. The material microstructure is described by a discrete valued random variable in each pixel. In order to generate this discrete valued random field, a Gaussian random field is first generated, and then converted to discrete valued form by a memoryless nonlinear transformation. The values of the Gaussian random field are generated in each pixel sequentially by conditioning on previously realized values.

3.4. Procedure

The domain on which a sample microstructure is to be generated is divided into hexagonal pixels as shown in Fig. 18. Pixelation of the domain allows the representation of the random field by the series of random variables Y_i, $i = 1, \ldots, n$ where n is the number of pixels in the domain. For the time being we allow the random field to be Gaussian with mean zero and unit variance, and allow it to have a covariance function given by $\rho(n_{nei})$, where

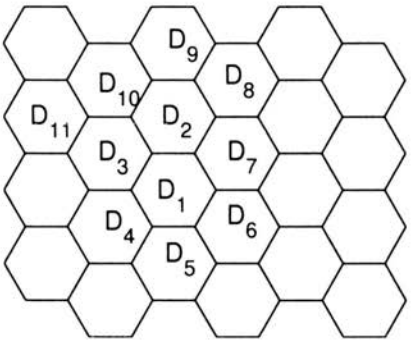

FIGURE 18. Hexagonal pixel geometry.

n_{nei} is the neighbor number of the pixels in question. For the covariance of a pixel with itself, $n_{nei} = 0$, with one of its neighbors $n_{nei} = 1$ for one of its neighbor's neighbors $n_{nei} = 2$ and so on.

The Gaussian random variables describing the random field are generated to match the target covariance function by generating the variables sequentially and conditioning on the variables which have already been realized. This procedure is best illustrated by an example.

Consider the pixel geometry given in Fig. 18, with the pixels labelled as shown. Let the random field to be generated, $Y(\mathbf{x})$, be Gaussian with mean zero and unit variance, and with covariance function $\rho(n_{nei}) = \rho^{n_{nei}}$. We begin by generating a realization y_1 of Y_1, the value of the random field in D_1, making use of the fact that $Y_1 \sim N(0,1)$.

We now define some quantities useful in describing the conditional distributions of the subsequent variables. The goal at each stage of the simulation is to generate a realization of the conditional Gaussian variable $[Y_i|\mathbf{Y}_c = \mathbf{y}_c]^T$, where $\mathbf{y}_c$ represents the values already generated, and is $n_c \times 1$ where n_c is the number of entries in the conditioning vector. The covariance matrix of $[Y_i, \mathbf{Y}_c^T]^T$ can be partitioned into

$$\begin{bmatrix} \rho_{ii} & \boldsymbol{\rho}_{ic} \\ \boldsymbol{\rho}_{ci} & \boldsymbol{\rho}_{cc} \end{bmatrix} \tag{3.7}$$

where $\boldsymbol{\rho}_{ic} = \boldsymbol{\rho}_{ci}^T$, and $\boldsymbol{\rho}_{cc}$ is $n_c \times n_c$. The conditional random variable Y_i is then Gaussian with mean $\mu = \boldsymbol{\rho}_{ic}\boldsymbol{\rho}_{cc}^{-1}\mathbf{y}_c$ and variance $\rho_{ii} - \boldsymbol{\rho}_{ic}\boldsymbol{\rho}_{cc}^{-1}\boldsymbol{\rho}_{ci}$.

Returning to the example, for $Y_2|Y_1 = y_1$, $\rho_{11} = 1$, $\boldsymbol{\rho}_{12} = \rho$, and $\boldsymbol{\rho}_{22} = 1$. These values, when substituted into the equations given above, yield the familiar result that Y_2 is normally distributed with mean ρy_1 and variance $1 - \rho^2$.

The sample generation proceeds sequentially until the entire domain has been filled. One issue with this procedure is that the vector of conditioning values $\mathbf{y}_c$ grows as the sample generation proceeds. In order to improve the efficiency of the process, the vector is truncated so that only those pixels which are neighbors with D_i are included. The truncated conditioning vector is denoted $\hat{\mathbf{y}}_c$ For example, for the generation of Y_{10}, the vector $\hat{\mathbf{y}}_c$ is $[y_2, y_8, y_9]^T$. The truncation can in principle be applied at longer distances. For example, one could condition on values in all second nearest neighbors, in which case $\hat{\mathbf{y}}_c$ for Y_{10} would be $[y_1, y_2, y_3, y_4, y_7, y_8, y_9]^T$. The tradeoff in the truncation decision is that between more accurate matching of the target covariance function and increased computational efficiency.

3.5. Non-Gaussian fields

The goal of this method is to generate realizations of discrete valued random fields representing n-phase composites. The marginal distributions of such fields are highly non-Gaussian, but can be matched by a translation mapping. Here, two- and three phase materials are modelled. The marginal density for a two phase composite, scaled so that it will have zero mean and unit variance, is

$$f(z) = \phi_1 \delta\left(z + \sqrt{\frac{1-\phi_1}{\phi_1}}\right) + (1-\phi_1)\delta\left(z - \sqrt{\frac{\phi_1}{1-\phi_1}}\right) \tag{3.8}$$

where ϕ_1 is the volume fraction of phase 1 and $\delta(\cdot)$ is the Dirac delta function. The corresponding distribution is

$$F(z) = \phi_1 H\left(-\sqrt{\frac{1-\phi_1}{\phi_1}}\right) + (1-\phi_1)H\left(\sqrt{\frac{\phi_1}{1-\phi_1}}\right) \tag{3.9}$$

where $H(\cdot)$ is the Heaviside function.

For a three phase material the density is

$$f(z) = \phi_1 \delta\left(z + \sqrt{\frac{\phi_2}{\phi_1\phi_2 + \phi_1^2}}\right) + (1-\phi_1-\phi_2)\delta(z) + \phi_2\delta\left(z - \sqrt{\frac{1}{\phi_1+\phi_2}}\right) \tag{3.10}$$

where ϕ_1 and ϕ_2 are volume fractions. The distribution is given by

$$F(z) = \phi_1 H\left(\sqrt{\frac{\phi_2}{\phi_1\phi_2 + \phi_1^2}}\right) + (1-\phi_1-\phi_2)H(0) + \phi_2 H\left(\sqrt{\frac{1}{\phi_1+\phi_2}}\right). \tag{3.11}$$

Using the above density and distribution functions it is possible to transform a sample of a Gaussian field generated using conditional distributions into a non-Gaussian field representing a two- or three-phase composite. Care must be taken, however, to ensure that the covariance function is matched correctly. If the target non-Gaussian covariance function is $\rho(n_{nei})$, then the covariance function $\rho_g(n_{nei})$ of the Gaussian image can be found by iteratively solving the inverse equation

$$\rho(n_{nei}) = \int_{-\infty}^{\infty}\int_{-\infty}^{\infty} g(u)g(v)\phi(u,v;\rho_g(n_{nei}))\,du\,dv \tag{3.12}$$

where $g(\cdot) = F^{-1} \circ \Phi(\cdot)$, $\Phi(\cdot)$ is the normal distribution, and $\phi(\cdot,\cdot;\rho)$ is the bivariate Gaussian density with correlation coefficient ρ.

For the two phase material with $\phi_1 = 0.25$, the covariance transformation is shown in Fig. 19. Strongly negative covariances cannot be replicated using this method.

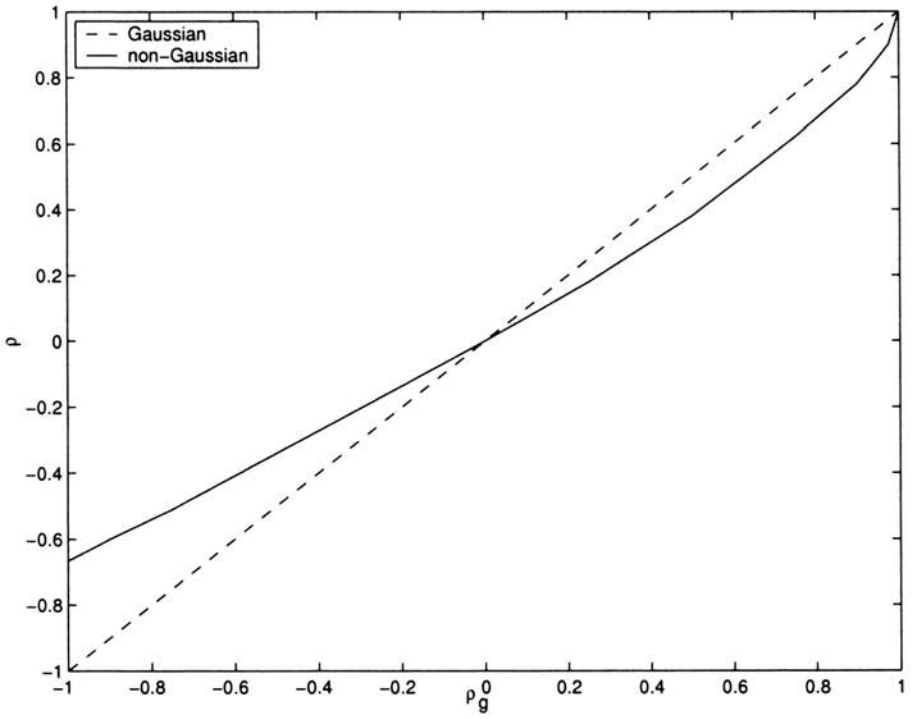

FIGURE 19. Covariance mapping for two phase material.

3.6. Two phase material

Realizations of a two phase material with volume fraction $\phi_1 = 0.5$ and covariance function $\rho^{n_{nei}}$ have been generated using the above procedures. Examples are shown below (Fig. 20) to demonstrate the flexibility of the method to generate microstructures with very different microstructures.

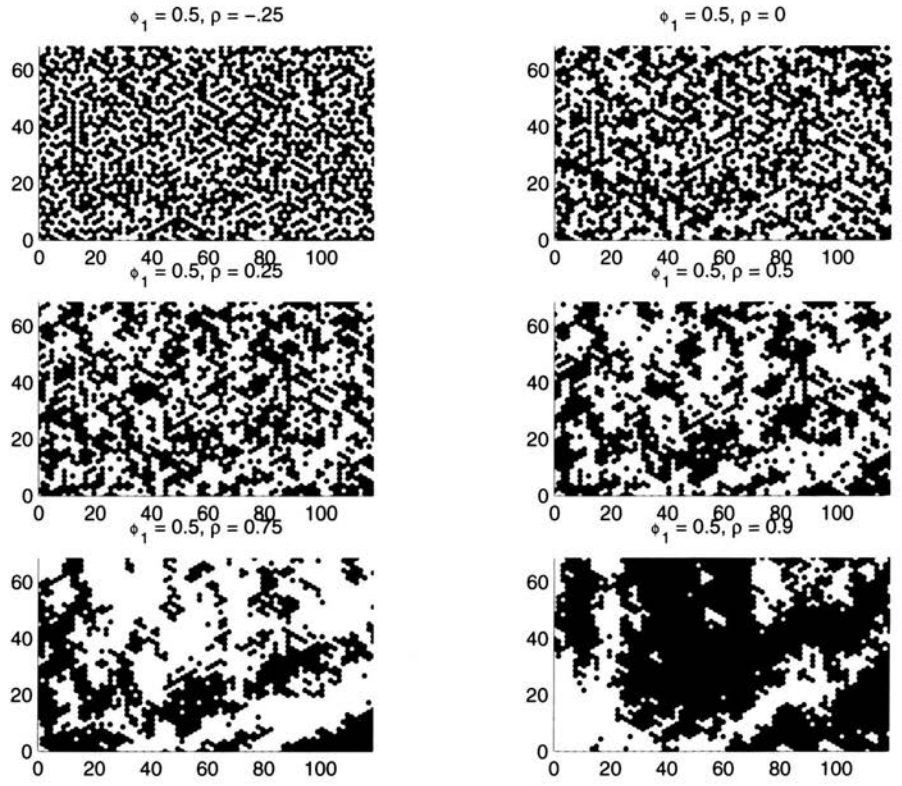

FIGURE 20. Example two phase materials.

Samples on a larger domain, with $\rho = 0.955$ and varying volume fractions are shown in Fig. 21

3.7. Three phase material

The procedure can also be used to generate realizations of three phase materials. The example shown in Fig. 22 has $\rho = 0.75$ and $\phi_1 = 0.5$, $\phi_2 = 0.23$.

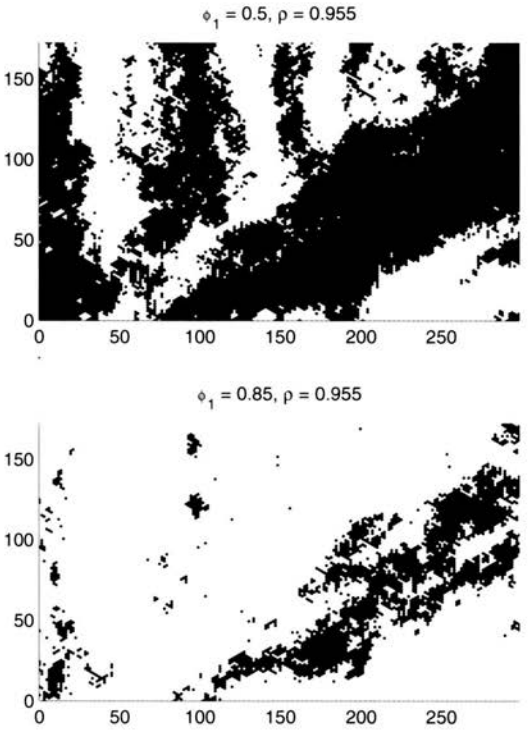

FIGURE 21. Example two phase materials.

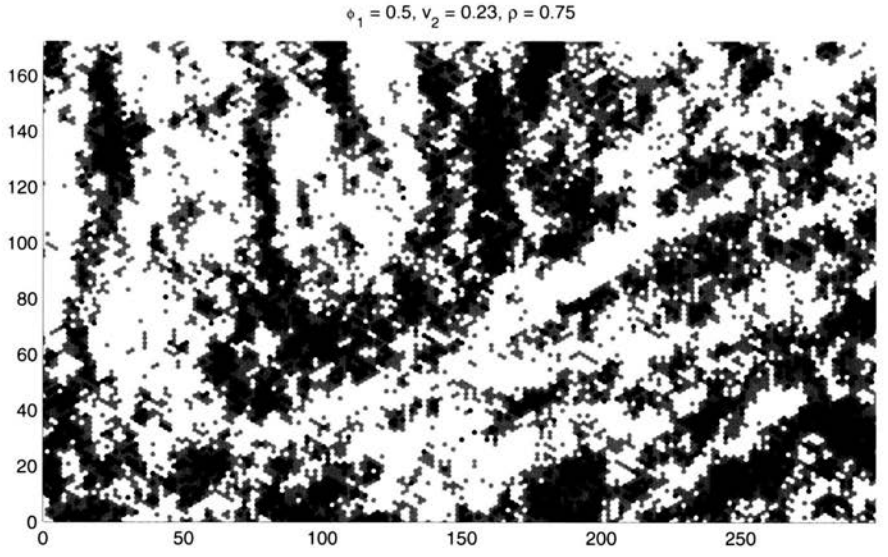

FIGURE 22. Example 3 phase materials.

4. Applications

We now give two example applications in which realizations of random heterogeneous materials are used to investigate the initiation and growth of microscale damage. In the first, a novel technique based on classification trees is used to identify the locations of likely crack initiation in a fiber reinforced composite. In the second, the statistical properties of random intergranular crack paths are determined using heuristic mechanical models and realizations of random polycrystalline grain structures.

4.1. Composite fracture

Fiber and particle reinforced composites have been one of the most studied forms of microstructured material. Attention has been paid both because of the range of application of the materials and because the microstructure of the materials lend themselves to analysis. The analysis is simplified by the deterministic nature of the reinforcement phase, which makes useful established methods such as the unit cell method. Statistical approaches are also often used for microstructure analysis [9, 16, 30]. While statistical approaches provide excellent results in such problems as the determination of effective material properties, the analysis of highly localized phenomena requires a different approach. The common approach is the use of high fidelity finite element analyses. This section describes a new method for efficiently characterizing random microstructures and provides a method for linking the characterization to material response. Details of the method are given in [24, 25]

4.1.1. Feature based microstructure characterization. Statistical characterizations of microstructures are typically *unsupervised*, that is, they are made without reference to the material response. Here we define a *supervised* characterization of the microstructure which makes use of *features* which are supervised in that they are geometric components of the microstructure which are associated with particular mechanical response. In this case the example microstructure is a cross section through a fiber reinforced composite and the response of interest is the location of crack initiation.

To generate these features, a set of n *training* microstructures is generated. The site of crack initiation for each of these microstructures under uniaxial tension is determined by analysis using a spring network model [29]. The microstructural geometry and boundary conditions are periodic. In order determine supervised features corresponding to fracture initiation, the geometry is shifted so that the crack initiation site as determined by the spring

network model is at the center of the microstructural sample. Every sample is discretized by an $m \times m$ mesh, so a vector with m^2 entries can be used to represent the microstructure with each entry being the average Young's modulus of the corresponding cell, $\mathbf{t}_i = [t_1, t_2, \ldots, t_{m^2}]^{\mathrm{T}}$, where $1 \leq i \leq n$. Let $\bar{\mathbf{t}}$ be the average of all $\mathbf{t}$'s, the training data set is expressed by the $m^2 \times n$ matrix $\mathbf{T} = [\mathbf{t}_1 - \bar{\mathbf{t}}, \mathbf{t}_2 - \bar{\mathbf{t}}, \ldots, \mathbf{t}_n - \bar{\mathbf{t}}]$. The covariance matrix is then defined as $\mathbf{C} = \mathbf{T}\mathbf{T}^{\mathrm{T}}$. According to the method of Principal Component Analysis (PCA), $\mathbf{C}$ can be decomposed as:

$$\mathbf{C} = \mathbf{F}\mathbf{D}\mathbf{F}^{\mathrm{T}} \tag{4.1}$$

where $\mathbf{D}$ is a diagonal matrix whose diagonal entires are the eigenvalues of $\mathbf{C}$ and $d_{11} \geq d_{22} \geq \cdots \geq d_{m^2 m^2} > 0$; $\mathbf{F} = [\mathbf{f}_1, \mathbf{f}_2, \ldots, \mathbf{f}_{m^2}]$ contains the corresponding eigenvectors and is orthonormal. The first r eigenvectors form a new base, $\mathbf{U} = [\mathbf{f}_1, \mathbf{f}_2, \ldots, \mathbf{f}_r]$, and is used to describe the microstructure instead of the original m^2-dimensional space. The transformed vector is obtained by

$$\mathbf{g}_i = \mathbf{U}(\mathbf{t}_i - \bar{\mathbf{t}}). \tag{4.2}$$

The above transform is called Karhunen-Loeve transform (KLT) and the new base vectors, $\mathbf{f}_1, \ldots, \mathbf{f}_r$, are the features used in our method.

On the contrary to the features obtained from above, another set of features are considered to account for the inclusion arrangement far away from the cracks. To find these features, the periodic boundaries are moved so that the crack initialization positions are on the four corners and the KLT procedure is repeated. In Fig. 23, two features are visualized which correspond to likely fracture initiation at the center of the microstructure for uniaxial ten-

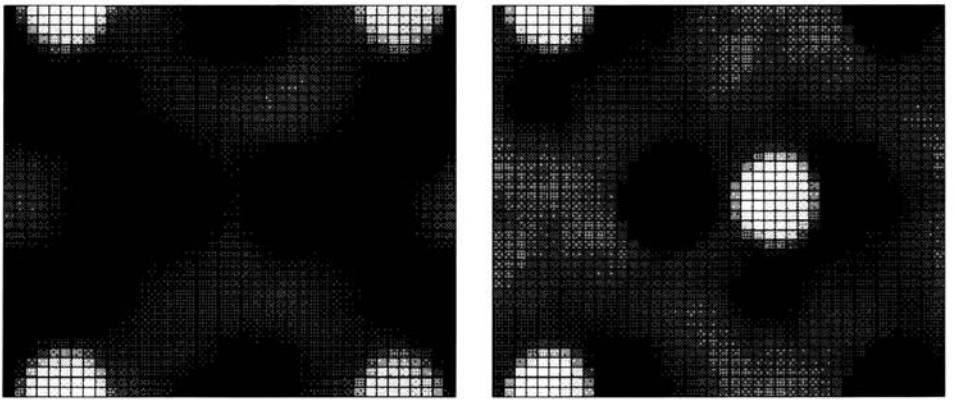

FIGURE 23. Visualization of features.

sion in the horizontal direction. In the plot, darker color represents a higher likelihood of finding an inclusion at that location.

4.1.2. Damage prediction using classification trees. The two types of features form a new space, *feature space*. A microstructure of the same size as the ones in the training data set can be described by projecting it to the feature space using Eq. (4.2), resulting in a vector, named *feature vector*, with a much lower dimensionality $2r$. The elements of this vector correspond to the strength of the various features in the example microstructure.

Bayesian classification trees [11] are constructed to determine, based on the elements of the feature vector, the likelihood of crack initiation in a specific microstructure. A Bayesian classification tree is a non-cyclic graph with nodes and edges. The nodes on the lowest level are called leaves and the highest level node is the root. Each node, except the root, has one and only one parent which is connected to it by an edge. Every non-leaf node is a feature criteria and every edge from the node indicates whether the feature criteria is satisfied or not. The leaves store probability values. Every path from the root to a leave is in fact a probability equation, designating the probability of a microstructure with all the feature criteria on the path having certain response. The feature criteria on a path thus constitute a *pattern*. We attempt to predict response of the microstructure by identifying these patterns in random microstructures.

Using Bayesian classification trees, three probability functions are established:

$$f_1(\mathbf{t}) \equiv Prob\,(\text{center crack}|g(\mathbf{t}))\,, \tag{4.3}$$

$$f_2(\mathbf{t}) \equiv Prob\,(\text{center crack}|g(\mathbf{t}))\,, \tag{4.4}$$

$$f_3(\mathbf{t}_i, \mathbf{t}_j) \equiv Prob\,(P_{cr}(\mathbf{t}_i) < P_{cr}(\mathbf{t}_j)|g(\mathbf{t}_i), g(\mathbf{t}_j))\,, \tag{4.5}$$

in which $g(\mathbf{t})$ is the feature values of microstructure $\mathbf{t}$; $P_{cr}(\mathbf{t})$ returns the fracture load. The classifier $f_3(\mathbf{t}_i, \mathbf{t}_j)$ compares the fracture load of two microstructures with center cracks.

With Eqs. (4.3), (4.4) and (4.5), the crack initialization position of a microstructural sample much larger than the training data is predicted using the following steps:

1. Use a moving window of the same size as the training microstructures and scan the window over the cross-section of the material;
2. For each position of the window, compute the feature vector of the microstructure covered by the window and determine the values of $f_1(\mathbf{t})$ and $f_2(\mathbf{t})$. If $f_1(\mathbf{t}) > p_1$ and $f_2(\mathbf{t}) < p_2$, store the window position as

a site of possible crack initiation, where p_1 and p_2 are the thresholds defined by the user;

3. Evaluate each pair of stored windows using function $f_3(\mathbf{t}_i, \mathbf{t}_j)$. The probability that the center of the ith window having the first crack of the whole material can be calculated by $\Pi_{j=1,\ldots,i-1,i+1,\ldots,k} f_3(\mathbf{t}_i, \mathbf{t}_j)$.

4.1.3. Example. In the example, the Young's modulus ratio between the inclusions and the matrix is $E_{in}/E_{mat} = 3$; the fracture stress ratio is $f_{in}/f_{mat} = 2$. Both the materials are ideal elastic brittle material. 600 microstructures with 20×20 mesh under uniaxial transverse tractions applied on the left and right boundaries are sampled for the training purpose. The training samples are used to calculate the features and set up the classification trees. These are then used to make predictions for the site of likely crack initiation in a larger sample with a 40×40 mesh. Figure 24 illustrates the example result. The shaded regions in Fig. 24(a) are the possible positions of the initial crack after (1) identification of sites of likely initiation, and (2) elimination of the subset of these sites which are at the center of windows with features corresponding to unlikely initiation; the three most likely position are then determined by the comparison function $f_3(\cdot)$ and are plotted in Fig. 24. Mechanics analysis is conducted for the whole material fracture initiates at the location which the classification site determined to be the most likely. Further Monte Carlo simulation indicates that the classification trees correctly predict the site of crack initiation with probability of approximately 0.50, and rank the site of crack initiation among the four most likely with probability approximately 0.80.

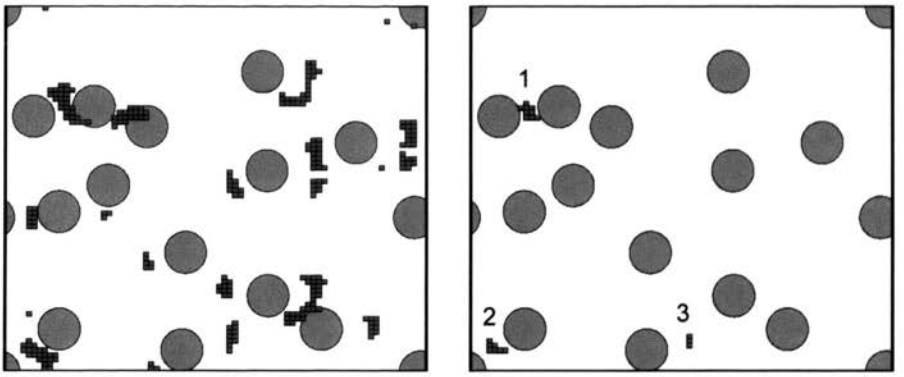

FIGURE 24. Example result.

4.2. Intergranular fracture

The probabilistic model developed for the microstructure and material properties of polycrystalline materials is not useful in an engineering context if it cannot be used to aid in the solution of important problems in probabilistic micromechanics. One such problem is the determination of the propagation paths and rates of microstructurally small cracks subject to possibly uncertain external actions, an issue which has received extensive study [36, 37, 3, 38, 13, 20, 8, 12, 39, 27]. The immense complexity of this problem places its detailed solution beyond the scope of this presentation, however, a simplified version of the problem is addressed to indicate the possible application of the probabilistic polycrystal model. It is recognized that the assumptions made detract from the physical realism of the analysis, yet, the solution does demonstrate the types of results which can be obtained using simulation based on the probabilistic polycrystal model [6].

Realizations of the random polycrystalline microstructure, generated using the procedure described above, are now used in an investigation of uncertainty in the trajectory of intergranular microcracks. The problem analyzed is shown in Fig. 25, namely a polycrystal subject to uniaxial tension with an initial edge crack along one of the grain boundaries.

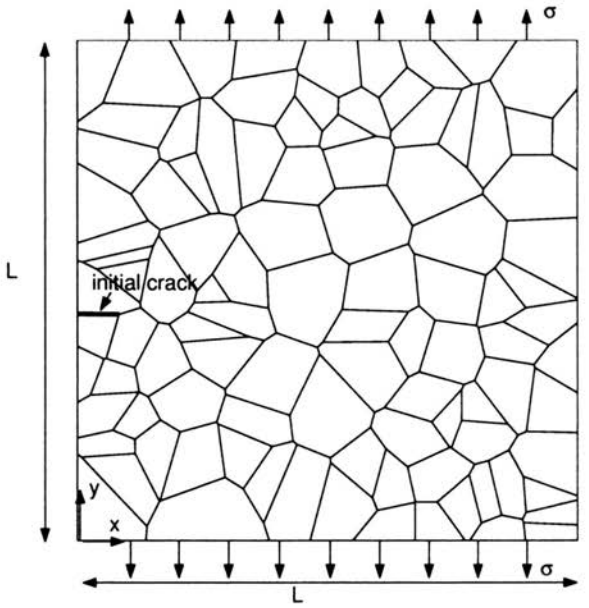

FIGURE 25. Schematic illustration of example crack propagation problem. A polycrystal subject to uniaxial tension.

By limiting the crack to an intergranular trajectory the number of possible crack trajectories is reduced from infinite to some finite, tractable number. A key result of the limitation to intergranular cracks is that only the relative resistance to fracture of the grain boundaries must be known, and not the resistance to fracture of the grain boundaries relative to the intragranular material. Several general assumptions are made regarding the behavior of the crack, namely:

- The crack propagates only along the grain boundaries–remains intergranular.
- The crack tip always proceeds in the direction of positive x_1.
- The crack does not branch.
- Propagation continues until the polycrystal is severed.

4.2.1. Crack path determination. Since the crack is restricted to the grain boundaries, the problem of determining the trajectory is reduced to that shown in Fig. 26; determination of which of two grain boundaries to proceed along when the crack tip encounters a grain boundary junction, or triple point. In the figure, the crack tip is at the junction of the grain boundaries separating grains p_1, p_2, and p_3. These grains have orientations $\mathbf{Y}_i$, $i = 1, 2, 3$, where the underscore in the figure indicates a vector quantity. The grain boundary between grains p_i and p_j is denoted by b_{ij} and has associated with it a misorientation angle θ_{ij} which is the angle part of the axis/angle representation of the misorientation between ψ_i and ψ_j. The dashed line, labelled homogeneous trajectory, indicates the trajectory along which the crack would propagate were it in a homogeneous continuum subject to the

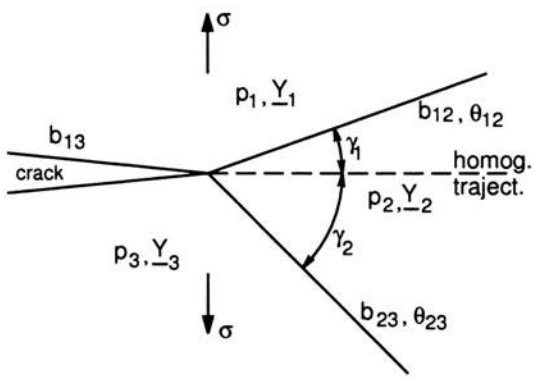

FIGURE 26. As an intergranular crack approaches a grain boundary junction (triple point), the crack must propagate along one of the candidate grain boundaries.

remote uniaxial stress σ. The angle between the homogeneous trajectory and b_{12} is γ_1 and γ_2 is the angle between the homogeneous trajectory and b_{23}.

While the grain boundary along which propagation occurs can be determined by energy considerations coupled with the principles of linear elastic fracture mechanics [7], the application of such a method requires extremely time consuming finite element analysis and Monte Carlo simulation. As yet, an insufficient number of simulations have been executed to allow any conclusions to be drawn regarding the propagation of uncertainty through the system.

Here, two mechanically simplified criteria are used to determine the crack direction at grain boundary junctions. In the first, which will be called the maximum misorientation criterion, the crack is assumed to propagate along the grain boundary which has the larger angle of misorientation, for example, along b_{23} in Fig. 26 if $\theta_{23} > \theta_{12}$. In the second, called the minimum deviation criterion, the crack propagates along the grain boundary which lies closest to the homogeneous trajectory. That is, the grain boundary for which the angle γ is minimized, which, in Fig. 26 is b_{12} since $\gamma_1 < \gamma_2$. These two criteria correspond, respectively, to the cases in which randomness in the crack trajectory is determined by randomness in the material properties or the grain geometry. The maximum misorientation criterion is motivated by the observation that grain boundaries with a high misorientation tend to have lower fracture toughness [21, 23]. The minimum deviation criterion is based on the intuition that, for an edge crack under uniaxial tension, the energy release per unit crack extension is greater the closer to perpendicular to the applied stress is the angle of propagation.

These two criteria are chosen in the belief that they represent extremes of the possible fracture behavior; the propagation depending either entirely upon the local material properties (maximum misorientation), or the local grain boundary geometry (minimum deviation). In both cases deviations in the local stress field are ignored. The physical reality likely is a combination of these two effects. As a preliminary attempt to address these intermediate cases, a mixed criterion is introduced. Define the quantity

$$\beta = W\frac{\theta}{\theta_{\max}} + (1 - W)\frac{\gamma - \gamma_{\max}}{\gamma_{\max}} \tag{4.6}$$

where $\theta_{\max} \approx 62°$ as given by the Mackenzie distribution [32], $\gamma_{\max} = 90°$ since the crack must always propagate forward, and W is a weight factor. When $W = 1$ the maximum misorientation criterion is obtained, and when $W = 0$ the minimum deviation criterion is obtained if the crack is assumed to propagate in the direction of greater β.

4.2.2. Monte Carlo simulation. To investigate the propagation of uncertainty in the material microstructure to uncertainty in intergranular crack trajectories Monte Carlo simulation was performed on the problem described above (see Fig. 25). Independent microstructural realizations were generated with the domain of the polycrystal being $S = [0, L]^2$. The crack is assumed to initiate at the grain boundary which intersects $x_1 = 0$ with x_2 coordinate closest to $x_2 = L/2$, and the crack tip is advanced using either the minimum deviation or maximum misorientation criterion until the crack tip encounters $x_1 = L$. The Monte Carlo simulation provides independent realizations of the random crack paths, denoted by $C(x)$. Figure 27 shows the crack paths de-

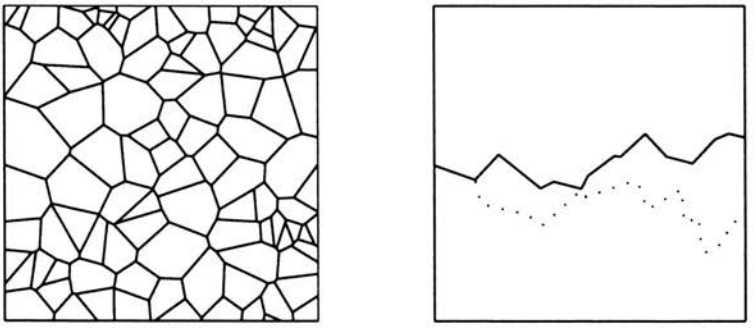

FIGURE 27. Single realization of intergranular crack growth using both the maximum misorientation and minimum deviation criteria. The solid line represents the minimum deviation criterion, and the dashed the maximum misorientation.

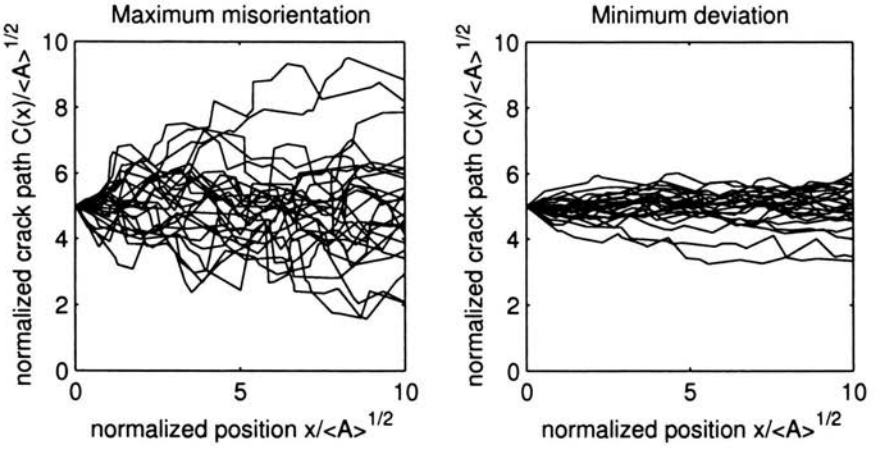

FIGURE 28. Monte Carlo simulation of intergranular crack growth using both the maximum misorientation and minimum deviation criteria.

termined for a sample microstructure using the two criteria, illustrating the significantly different crack paths obtained by the two methods.

Figure 28 shows 25 crack path realizations for each criterion. The domain of the samples, with $L = 500\,\mu$m, is $S = [0, 500]^2\,\mu$m with an average of 100 grains. Two adjustments are made to the crack paths as presented in Fig. 27: the crack paths are normalized using $\tilde{x} = x/\sqrt{\bar{A}}$ and $\tilde{C}(x) = C(x)/\sqrt{\bar{A}}$, where $\bar{A}$ is the average grain area, and the initial crack path is shifted so that $C(0)/\sqrt{\bar{A}} = 5$. The normalization is applied so that statistics of the crack paths can be computed non-dimensionally and to neglect uncertainty in the initiation site of the crack. The side by side comparison of crack paths obtained by the two different criteria indicate that the minimum deviation criterion results in crack paths much closer to the homogeneous trajectory than those obtained by use of the maximum misorientation criterion.

This observation is confirmed by the statistics shown in Fig. 29. The variance of $\tilde{C}(\tilde{x})$ is linear in $\tilde{x}$. The growth rates of the variance are 0.50 and 0.15 with respect to $\tilde{x}$ for the maximum misorientation and minimum deviation criteria respectively.

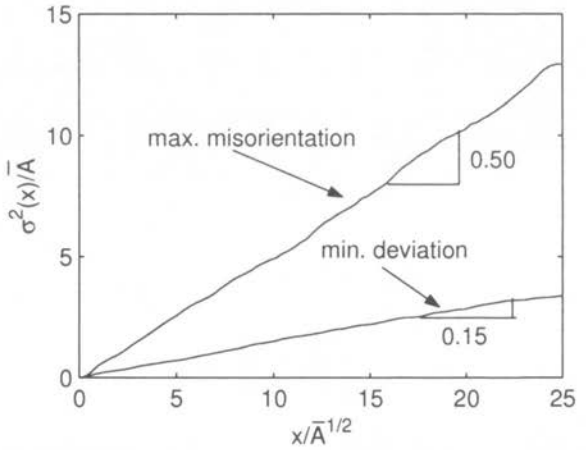

FIGURE 29. Growth of variance of the crack trajectories.

Example calculations with the mixed criterion yield some interesting preliminary results. When $W = 0.25$, the crack path has a variance growth rate of 0.35, when $W = 0.5$ the variance growth rate is 0.21, and when $W = 0.75$ the variance growth rate is 0.17. These variance growth rates, corresponding to intermediate values of the criterion weight, demonstrate the nonlinear sensitivity of the variance growth to the weight, and also that the minimum deviation criterion appears to dominate for weights close to 1. It is in this

regime of intermediate weights that the true behavior of intergranular cracks is expected to be found. Through the use of higher fidelity, but more time consuming mechanical models, future investigation will attempt to further understanding of the behavior of intergranular cracks in this intermediate regime.

4.2.3. Probabilistic model. The random nature of the crack paths generated by Monte Carlo simulation, coupled with the observed linear variation of the crack path variance suggests that a scaled Brownian motion may be an appropriate model for intergranular crack trajectories. Let the normalized crack be a random process defined by

$$\tilde{C}(\tilde{x}) = \sigma B(\tilde{x}) \tag{4.7}$$

where $B(\tilde{x})$ is a standard normal Brownian motion process, that is, a Gaussian process with stationary independent increments such that $B(u+h) - B(u)$, $h > 0$ is $N(0,h)$. The process $\tilde{C}(\tilde{x})$ has zero mean and variance $\text{var}(\tilde{C}(\tilde{x})) = \sigma^2\tilde{x}$ if $\text{var}(\tilde{C}(0)) = 0$. The parameter σ is determined to be $\sqrt{0.50}$ and $\sqrt{0.15}$ for the cases of cracks whose trajectory is determined by the maximum misorientation and minimum deviation criteria respectively.

To generate realizations of intergranular crack paths a step size $\Delta\tilde{x}$ is selected which is equal to 1. An initial condition $\tilde{C}(0)$ is chosen and the crack trajectory is generated by the forward difference equation

$$\tilde{C}(\tilde{x}_{i+1}) = \tilde{C}(\tilde{x}_i) + \sigma\sqrt{\Delta\tilde{x}}\, A_i, \tag{4.8}$$

where the A_i's are independent standard normal Gaussian random variables. Samples of this process are shown in Fig. 30 for both values of the calibration parameter. The sample trajectories bear a qualitative resemblance to the simulated trajectories of Fig. 28 and match the linear growth of variance. The process can then be rescaled to actual units by $C(x) = \tilde{C}(x/\sqrt{\bar{A}})\sqrt{\bar{A}}$. This simulation method can as well be applied to generate crack trajectories corresponding to the mixed propagation criterion introduced earlier. It entails simply finding the value of the variance growth rate for the desired value of W, and inserting this value into Eq. (4.8).

This example illustrates the possibility of using Monte Carlo simulation of microstructural evolution as a means of generating statistics on microstructural features such as crack trajectories. If sufficient confidence can be placed in the mechanics of the models used in the Monte Carlo simulation then direct probabilistic modelling of the evolved microstructures may be possible, allowing generation of sample microstructures at the desired stage of evolution. While the mechanics of the crack propagation models presented here

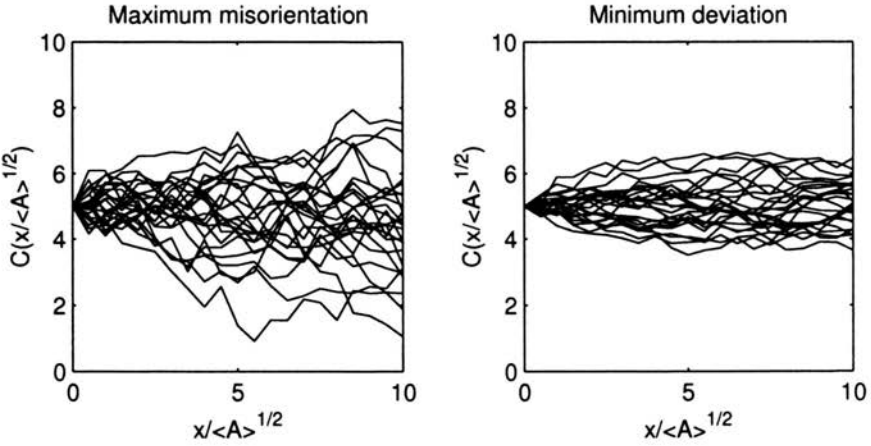

FIGURE 30. Realizations of crack trajectories generated from scaled Brownian motion model for intergranular cracks.

are too simplified to offer such a claim to physical reality, the example serves to illustrate the method, and the potential usefulness of the described probabilistic model of polycrystalline microstructures.

5. Summary

These presentations have had three main goals:

1. to introduce the types of statistical quantities which can be obtained from data to characterize random microstructures;
2. to demonstrate the possibility of developing probabilistic models for random heterogeneous materials which can efficiently generate samples which match the target statistics of real materials;
3. to show, by examples, the possible application of realizations from such probabilistic models for analysis of small scale fracture in random microstructures.

In each of these areas, there has necessarily been a great deal left out. In characterization and statistics there remains much to be said and discovered about higher order statistics of random microstructures and methods of characterizing features such as phase connectivity. Also, the issue of quantifying grain shape is a non-trivial one which deserves further attention. With respect to modelling of polycrystalline microstructures, the two part model is perhaps less preferable than one which directly generates the discontinuous samples of the orientation field. This represents a significant challenge

both in calibration of the field and sample generation. Much work remains in modelling of multi-phase materials, particularly with regard to efficiency of algorithms and methods of matching higher order statistics of the measured material. While the application example demonstrates the type of analyses possible with access to probabilistic material models, increased computational power should allow the incorporation of higher fidelity mechanics to the analysis, resulting in the possibility of analyses which are predictive of real material behavior. The material presented is intended as an indication of ongoing research in several of the areas of random microstructure simulation and analysis. The importance of random behavior at the microscale is one of the large challenges awaiting the engineering community with respect to structures and systems of all scales.

Acknowledgements

The author would like to thank those that have collaborated in the research presented here, especially Professor M. Grigoriu of Cornell University. Also due thanks are Professor A. Ingraffea, and Professors P. Dawson and M.P. Miller, also of Cornell University. Professor T. Igusa of Johns Hopkins University guided the research in Bayesian classification, and graduate student H. Liu worked out many of the details. Professor G. Deodatis of Columbia University graciously provided the figures for the description of his method for simulating multi-phase composites using level crossings of random processes. Financial support for some of the work presented was provided by AFOSR grant #F49620-98-1-0401.

References

1. B. L. ADAMS, Orientation imaging microscopy: Application to the measurement of grain boundary structure, *Materials Science and Engineering A*, Vol. A166, pp. 59–66, 1993.
2. B. L. ADAMS, P. I. ETINGHOF, and D. D. SAM, Coordinate free tensorial representation of n-point correlation functions for microstructure by harmonic polynomials, in: *Proceedings of the 10th International Conference on Textures and Materials, September 20-24, 1993 Clausthal, Germany*, Aedermannsdorf, Switzerland: Trans Tech Publishers, 1994, pp. 287–294.
3. P. M. ANDERSON and J. R. RICE, Constrained creep cavitation of grain boundary facets, *Acta Metallurgica*, Vol. 33, pp. 409–422, 1985.
4. S. R. ARWADE, Stochastic characterization and simulation of material microstructures with application to aluminum, Ph.D. dissertation, Cornell University, Ithaca, NY, January 2002.
5. S. R. ARWADE and M. GRIGORIU, A model for non-stationary and anisotropic polycrystalline microstructures, in: *Proceedings of the 9th International Conference on*

Applications of Statistics and Probability in Civil Engineering, San Francisco, CA: Millpress, July 2003.

6. S. R. ARWADE and M. GRIGORIU, A probabilistic model for polycrystalline microstructures with application to intergranular fracture, *ASCE Journal of Engineering Mechanics*, 2003 (Accepted for publication).
7. S. R. ARWADE, M. GRIGORIU, and A. R. INGRAFFEA, Crack growth in stochastic microstructures, in: *Stochastic Structural Dynamics: Proceedings of the Fourth International Conference on Stochastic Structural Dynamics*, Notre Dame, IN, August 1998.
8. R. BALLARINI, R. L. MULLEN, Y. YIN, H. KAHN, S. STEMMER, and A. H. HEUER, The fracture toughness of polysilicon microdevices: A first report, *Journal of Materials Research*, Vol. 12, pp. 915–922, 1997.
9. S. C. BAXTER and L. L. GRAHAM, Characterization of random composites using moving-window technique, *Journal of Engineering Mechanics*, Vol. 126, No. 4, pp. 389–397, April 2000.
10. J. R. BENJAMIN and C. A. CORNELL, *Probability, Decision and Statistics for Civil Engineers*, New York: McGraw-Hill, 1970.
11. W. BUNTINE, Learning classification tree, *Statistics and Computing*, Vol. 2, pp. 63–73, 1992.
12. P. D. CHINH, Asymptotic estimates on scatter ranges for elastic properties of completely random polycrystals, *Physica B: Condensed Matter*, Vol. 334, No. 1-2, pp. 98–111, 2003.
13. P. R. DAWSON, Computational crystal plasticity, *International Journal of Solids and Structures*, Vol. 37, pp. 115–130, 2000.
14. G. DEODATIS and S. KOUTSOURELAKIS, A methodology to generate sample realizations of two-phase random media, in: *Fifth World Congress on Computational Mechanics*, Vienna, Austria, 2002.
15. J. L. DEVORE, *Probability and Statistics for Engineering and the Sciences*, Pacific Grove, CA: Brooks/Cole, 1991.
16. R. K. EVERETT and J. M. CHU, Modeling of non-uniform composite microstructure, *Journal of Composite Materials*, Vol. 27, pp. 1128–1144, 1993.
17. M. GRIGORIU, Crossing of non-Gaussian translation processes, *Journal of Engineering Mechanics, ASCE*, Vol. 110, No. 4, pp. 610–620, 1984.
18. M. GRIGORIU, *Applied non-Gaussian Processes: Examples, Theory, Simulation, Linear Random Vibration and MATLAB Solutions*, Englewood Cliffs, NJ: Prentice–Hall, 1995.
19. M. GRIGORIU, O. DITLEVSEN, and S. R. ARWADE, A Monte Carlo simulation model for stationary non-Gaussian processes, *Probabilistic Engineering Mechanics*, Vol. 18, pp. 87–95, 2003.
20. J. W. HUTCHINSON, Bounds and self-consistent estimates for creep of polycrystalline materials, *Proceedings of the Royal Society of London A*, Vol. 238, pp. 101–127, 1976.
21. H. KURISHITA, S. KUBA, H. KUBO, and H. YOSHINGA, Misorientation dependance of grain boundary fracture in molybdenum bicrystals with various ⟨110⟩ twist boundaries, *Transactions of the Japan Institute of Metals*, Vol. 26, pp. 332–240, 1985.

22. E. N. LANDIS, E. N. NAGY, and D. T. KEANE, Microstructure and fracture in three dimensions, *Engineering Fracture Mechanics*, Vol. 70, No. 7, pp. 911–925, 2003.

23. G. H. LI and L. D. ZHANG, Relationship between misorientation and bismuth induced embrittlement of [001] tilt boundary in copper bicrystal, *Scripta Metallurgica et Materialia*, Vol. 32, pp. 1335–1340, 1995.

24. H. LIU, S. R. ARWADE, and T. IGUSA, Random composites characterization and damage estimation using a classifier model, in: *Proceedings of the 16th Engineering Mechanics Conference*, Seattle, WA: ASCE, July 2003.

25. H. LIU, T. IGUSA, and S. R. ARWADE, Random composites characterization and damage estimation using a classifier model, *Computers and Structures*, 2004 (Submitted).

26. D. MIKA, Personal communication, 1997.

27. A. NEEDLEMAN, R. J. ASARO, J. LEMOND, and D. PIERCE, Finite element analysis of crystalline solids, *Computational Methods in Applied Mechanics and Engineering*, Vol. 52, pp. 689–708, 1985.

28. K. OKAZAKI and H. CONRAD, Grain size distribution in recrystallized alpha-titanium, *Transactions of the Japan Institute of Metals*, Vol. 13, pp. 198–204, 1972.

29. M. OSTOJA-STARZEWSKI, Damage in a random microstructure, in: *Applied Mechanics Reviews: Pan American Congress of Applied Mechanics*, Vol. 42, ASME, 1989, p. s202.

30. R. PYRZ, Topological disorder of microstructure and its relation to the stress field, *Int. J. Solids Structures*, Vol. 35, No. 19, pp. 2413–2427, 1998.

31. www.qhull.org, internet resource.

32. V. RANDLE, *The Measurement of Grain Boundary Geometry*, Bristol, UK: Institute of Physics, 1993.

33. T. T. SOONG and M. GRIGORIU, *Random Vibrations of Mechanical and Structural Systems*, Englewood Cliffs, NJ: Prentice Hall, 1993.

34. D. STOYAN, W. S. KENDALL, and J. MECKE, *Stochastic Geometry and its Applications*, Chichester, England: Wiley, 1995.

35. S. TORQUATO, *Random Heterogeneous Materials: Microstructure and Macroscopic Properties*, New York: Springer, 2002.

36. E. VAN DER GIESSEN and V. TVERGAARD, Effect of random variations in microstructure on the development of final creep failure in polycrystalline aggregates, *Modelling Simul. Mater. Sci. Eng.*, Vol. 2, pp. 721–738, 1994.

37. E. VAN DER GIESSEN and V. TVERGAARD, Interaction of cavitating grain boundary facets in creeping polycrystals, *Mechanics of Materials*, Vol. 17, pp. 47–69, 1994.

38. D. S. WILKINSON, The effect of a non uniform void distribution on grain boundary void growth during creep cavitation, *Acta Metallurgica*, Vol. 36, pp. 2055–2063, 1988.

39. M. S. WU and J. GUO, Analysis of a sector crack in a three dimensional voronoi tessellation with microstructural stresses, *Journal of Applied Mechanics*, Vol. 67, No. 1, pp. 50–58, 2000.